NEA/NSC/DOC(95)10
INDC(Ger)-040
Jül-3086

PROGRESS REPORT ON NUCLEAR DATA RESEARCH IN THE FEDERAL REPUBLIC OF GERMANY

for the Period April 1, 1994 to March 31, 1995

July 1995

Edited by
S. M. Qaim
Forschungszentrum Jülich GmbH
Institut für Nuklearchemie
Jülich, Federal Republic of Germany

FOREWORD

As in previous years, this report has been prepared to promote the exchange of nuclear data research information between the Federal Republic of Germany and other member states of OECD/NEA and IAEA. It covers progress reports from the research centres at Karlsruhe and Jülich, the universities of Dresden, Hannover, Köln, Mainz, Marburg as well as from PTB Braunschweig. The emphasis in the work reported here is on measurement, compilation and evaluation of nuclear data for pure and applied science programmes, such as those relevant to fission- and fusion-reactor technology, accelerator shielding and development, astrophysics research, cosmogenic and meteoritic investigations, production of medically important radioisotopes, etc.

The coordination of nuclear data activities at the international level is done by two committees: the NEA-Nuclear Science Committee (NEA-NSC) and the IAEA-International Nuclear Data Committee (INDC). The present Editor has the privilege and the responsibility of representing Germany in both the committees. This report thus serves also as a background information to those committees.

Each contribution is presented under the laboratory heading from where the work is reported. The names of other participating laboratories are also mentioned. When the work is relevant to the World Request List for Nuclear Data, WRENDA 93/94 (INDC(SEC)-104/U+G), the corresponding identification numbers are given.

S.M. Qaim

Jülich, July 1995

CONTENTS

PHYSIKALISCH-TECHNISCHE BUNDESANSTALT BRAUNSCHWEIG

FORSCHUNGSZENTRUM KARLSRUHE
INSTITUT FÜR KERNPHYSIK

1. STELLAR NEUTRON CAPTURE CROSS SECTIONS OF THE Ba ISOTOPES*

F. Voß, K. Wisshak, K. Guber, F. Käppeler, G. Reffo[1]

The neutron capture cross sections of ^{134}Ba, ^{135}Ba, ^{136}Ba, and ^{137}Ba were measured in the energy range from 5 to 225 keV . Neutrons were produced via the ^{7}Li(p,n)^{7}Be reaction by bombarding metallic Li targets with a pulsed proton beam. Capture events were registered with the Karlsruhe 4π BaF_2 detector. The cross section ratios were determined with an overall uncertainty of ~3%, an improvement by factors of five to eight compared to existing data. Severe discrepancies were found with respect to previous results. As a new possibility in time of flight experiments, isomeric cross section ratios could be determined for ^{135}Ba, ^{136}Ba, and ^{137}Ba. Maxwellian averaged neutron capture cross sections were calculated for thermal energies between kT = 10 keV and 100 keV. These stellar cross sections were used in an s–process analysis. For the s–only isotopes ^{134}Ba and ^{136}Ba the $N_s < \sigma >$ ratio was determined to 0.875±0.025. Hence, a significant branching of the s–process path at ^{134}Cs can be claimed for the first time, in contrast to predictions from the classical approach. This branching yields information on the s–process temperature, indicating values around T_8=2. The new cross sections are also important for the interpretation of barium isotopic anomalies, which were recently discovered in SiC grains of carbonaceous chondrite meteorites. Together with the results from previous experiments on tellurium and samarium, a general improvement of the $N_s < \sigma >$ systematics in the mass range A=120–150 is achieved. This yields a more reliable separation of s– and r–process contributions for comparison with stellar observations, but reveals a 20% discrepancy with respect to the solar barium abundance.

*Phys. Rev. C **50** (1994) 2582

2. RESONANCE NEUTRON CAPTURE IN ^{136}Ba

F. Voß, K. Wisshak, F. Käppeler

The neutron capture cross section of ^{136}Ba, which was determined recently with the Karlsruhe 4π BaF_2 detector, has been reanalyzed in the low energy region using a shape analysis program. Parameters of 45 resonances were extracted which allow a more reliable

[1]ENEA, Laboratorio Dati Nucleari, Viale Ercolani 8, I–40138 Bologna, Italy

Table 1: Maxwellian averaged neutron capture cross sections of ^{136}Ba

Thermal energy kT (keV)	$<\sigma v>/v_T$ (mbarn)[a] This Work	Voss *et al* [b]
10	109.7 ± 4.6	114.9 ± 6.5
12	99.3 ± 3.9	103.5 ± 5.2
20	74.9 ± 2.7	77.4 ± 3.0
25	66.5 ± 2.3	68.4 ± 2.5
30	60.6 ± 2.1	62.0 ± 2.1

[a] With total uncertainties
[b] F. Voß, K. Wisshak, K. Guber, F. Käppeler, G. Reffo 1994, *Phys. Rev. C* **50** 2582

determination of the averaged cross section below 20 keV. The results confirm our first analysis and the reported stellar cross section as illustrated by the comparison in Table 1. Accordingly, the results of the s–process studies based on these data remain unchanged.

3.NEUTRON CAPTURE CROSS SECTIONS OF THE CERIUM ISOTOPES FOR s– and p–PROCESS STUDIES

F. Käppeler, K. A. Toukan[1], M. Schumann , A. Mengoni[2]

The neutron capture cross sections of the stable cerium isotopes 136, 138, 140, and 142 have been measured relative to that of gold by means of the activation method. The samples were irradiated in a quasi–stellar neutron spectrum for $kT = 25$ keV using the ^{7}Li(p,n)^{7}Be reaction near threshold. Variation of the experimental conditions in different activations and the use of different samples allowed for the reliable determination of corrections and the evaluation of systematic uncertainties. Figure 1 shows the γ–ray spectrum measured after one of these activations, where the irradiation and counting times were chosen in such a way that it exhibits the γ–ray transitions associated with the decay of *all* cerium isotopes.
The resulting stellar cross sections can be given with uncertainties between 3% and 7%. The experimental results are complemented by a set of calculated cross sections for the unstable isotopes from ^{132}Ce to ^{141}Ce. The present data for ^{136}Ce and ^{138}Ce are the first experimental information in this mass region of relevance for p–process studies, whereas the neutron rich isotopes beyond ^{140}Ce are important for an update of the s–process flow in the Ce–Pr–Nd region including the branchings at ^{141}Ce and ^{142}Pr. In this context, the new ^{142}Ce cross section allows to resolve a discrepany in previous data. The improved s–abundances are also used for a discussion of r– and p–process residuals.

[1]College of Engineering and Technology, The University of Jordan, Amman, Jordan
[2]ENEA, Laboratorio Dati Nucleari, Viale Ercolani 8, I–40138 Bologna, Italy

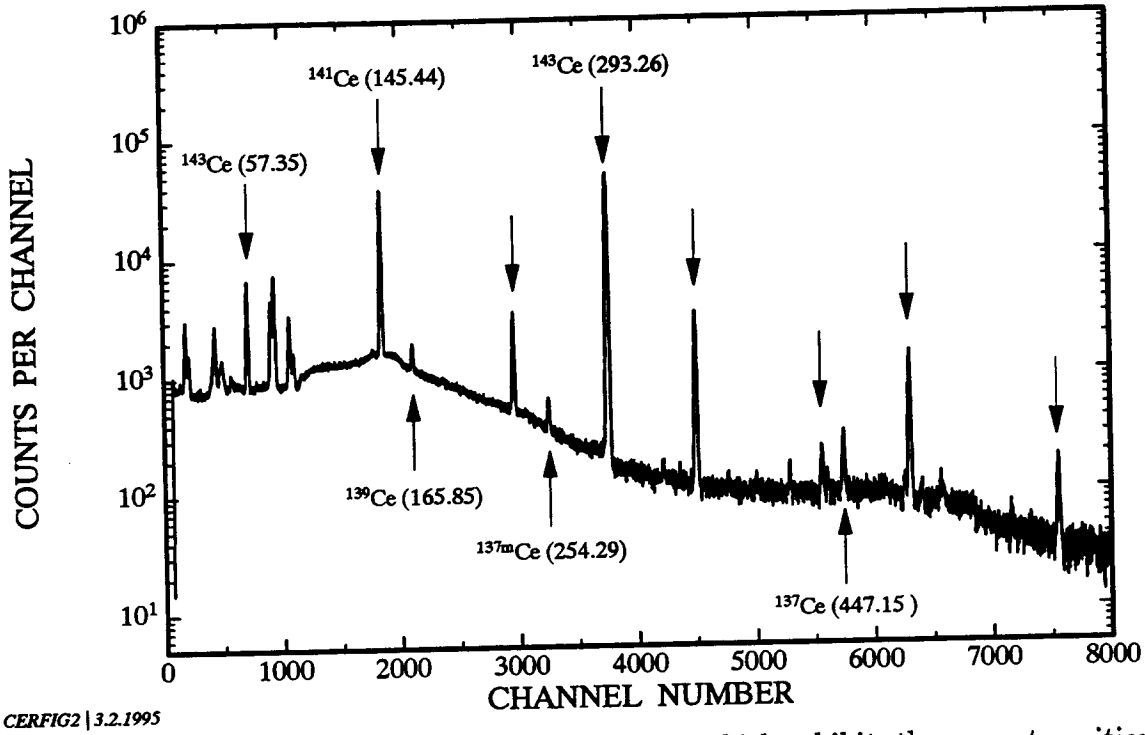

Fig.1. The γ–ray spectrum measured after activation, which exhibits the γ–ray transitions from the decay of all cerium isotopes. The dominant lines which were used to evaluate the respective cross sections are indicated by arrows (γ–energies in keV).

4. STELLAR NEUTRON CAPTURE CROSS SECTIONS OF Nd, Pm, AND Sm ISOTOPES*

K. A. Toukan[1], K. Debus[2], F. Käppeler, G. Reffo[3]

The neutron capture cross sections of ^{146,148,150}Nd have been determined relative to that of gold by means of the activation method. The samples were irradiated in a quasi–stellar neutron spectrum for kT = 25 keV using the ^{7}Li(p,n)^{7}Be reaction near threshold. Variation of the experimental conditions in different activations and the use of different samples allowed to determine the necessary corrections and to evaluate systematic uncertainties quantitatively. The resulting stellar cross sections can be given with uncertainties of 6%, which represents a considerable improvement compared to previous measurements. These data are complemented by a new set of calculated cross sections for the unstable isotopes ^{147}Nd, ^{147,148,149}Pm, and ^{151}Sm, which act as branching points in the s–process path. Based on these results, the s–process flow in the Nd-Pm-Sm region is discussed with respect to the neutron density during stellar helium burning and to isotopic anomalies in meteorites, The updated s–abundances are also used for a discussion of r– and p–process residuals.

*Phys. Rev. C 51 (1995) 1540

[1]College of Engineering and Technology, The University of Jordan, Amman, Jordan
[2]University of Heidelberg
[3]ENEA, Laboratorio Dati Nucleari, Viale Ercolani 8, I–40138 Bologna, Italy

5. STELLAR (n,γ) CROSS SECTIONS OF THE UNSTABLE ISOTOPE ^{155}Eu*

S. Jaag, F. Käppeler

The stellar (n,γ) cross section of the comparably short-lived isotope ^{155}Eu ($t_{1/2}$ = 4.96 yr) has been experimentally determined relative to that of gold by means of the activation method. A sample containing only 3.4×10^{14} ^{155}Eu atoms was irradiated for 17 days in a quasi-stellar neutron spectrum corresponding to a thermal energy of kT = 25 keV. The cross section obtained from the induced activity yields $<\sigma v>/v_T$ = 1320±84 mb at kT = 30 keV. This result is of relevance for analyzing the abundance pattern in the s-process branchings at A = 151, 152, and 154 with respect to the temperature during helium shell burning in low mass stars.

*Phys. Rev. C 51 (June 1995)

6. STELLAR (n,γ) CROSS SECTIONS OF THE GADOLINIUM ISOTOPES*

K. Wisshak, F. Voß, F. Käppeler, K. Guber[1], L. Kazakov[2], N. Kornilov[2], M. Uhl[3], G. Reffo[4]

The neutron capture cross sections of ^{152}Gd, ^{154}Gd, ^{155}Gd, ^{156}Gd, ^{157}Gd, and ^{158}Gd were measured in the energy range from 3 to 225 keV at the Karlsruhe 3.75 MV Van de Graaff accelerator. Neutrons were produced via the ^{7}Li(p,n)^{7}Be reaction by bombarding metallic Li targets with a pulsed proton beam. Capture events were registered with the Karlsruhe 4π Barium Fluoride Detector, which was improved by replacing crystals with high α background and by introducing a pierced crystal at zero degrees with respect to the beam axis. These changes resulted in a significantly increased efficiency for capture events. The main experimental problem was that the samples of the two s-isotopes ^{152}Gd and ^{154}Gd showed only relatively low enrichment. Nevertheless, the spectroscopic quality of the BaF_2 detector allowed to evaluate the corresponding corrections for isotopic impurities reliably. The cross section ratios could be determined with an overall uncertainty of typically 1%, an improvement by factors of five to ten compared to existing data. Severe discrepancies were found with respect to previous results. Maxwellian averaged neutron capture cross sections were calculated for thermal energies between kT = 10 keV and 100 keV. For the common s-process thermal energy of kT = 30 keV, the present results are compared with previous evaluations in Table 2.

The new stellar cross sections were used for an updated analysis of the s-process reaction flow in the mass region between samarium and gadolinium, which is characterized

[1]now at Oak Ridge National Laboratory, USA
[2]IPPE Obninsk, Russia
[3]University of Vienna, Austria (deceased)
[4]ENEA, Centro Dati Nucleari, Bologna

Table 2: Maxwellian averaged cross sections at kT=30 keV compared to previous evaluations

Isotope	Present results (mbarn)[a]	Evaluations	
		Bao and Käppeler[b]	Beer, Voss, and Winters[c]
^{152}Gd	1049 ± 17	985 ± 61	1045 ± 65
^{154}Gd	1028 ± 12	1278 ± 102	878 ± 27
^{155}Gd	2648 ± 30	2800 ± 280	2721 ± 90
^{156}Gd	615.2 ± 5.1	639 ± 64	639 ± 64
^{157}Gd	1369 ± 15	1538 ± 154	1355 ± 39
^{158}Gd	323.6 ± 2.8	208 ± 19	221 ± 20

[a] The 1.5% uncertainty of the gold cross section is not included here, since it cancels out in most applications of relevance for nuclear astrophysics.
[b] Z.Y. Bao and F. Käppeler 1987, *At. Data Nucl. Data Tables* **36**, 411
[c] H. Beer, F. Voss, and R.R. Winters 1992, *Ap. J. Suppl.* **80**, 403

by branchings at ^{151}Sm, ^{154}Eu, and ^{155}Eu. With the classical approach, the s-process temperature could be constrained corresponding to a range of thermal energies between kT=28 keV and 33 keV. The ^{152}Gd production in low mass stars was found to depend strongly on the neutron freeze-out at the end of the helium shell burning episodes.

* Report FZKA-5510, Forschungszentrum Karlsruhe (May 1995)

FORSCHUNGSZENTRUM KARLSRUHE INSTITUT FÜR NEUTRONENPHYSIK UND REAKTORTECHNIK

Nuclear Data Evaluation

1. Cross Section Fluctuations and Self-Shielding in Structural Materials

F.H. Fröhner

Recent transmission measurements on iron, nickel and chromium performed at Geel and Oak Ridge with very high resolution have shown that pronounced resonance structure extends far into the unresolved resonance region (better: the region of nonanalysed resonances). The structure thus observed in the total cross section implies similar, positively correlated structure for all partial cross sections. It is therefore not correct to neglect all fluctuations of the cross sections for elastic and inelastic scattering in the "unresolved" resonance region and the concomitant self-shielding effects on neutron transport, activation and transmutation, as has often been done in the past.

At what energies self-shielding becomes negligible can be seen as follows. The transmission of collimated neutrons through a slab of aereal thickness n can be expressed in terms of the mean and the higher moments of the cross section distribution by the cumulant expansion

$$\begin{aligned}\langle \exp(-n\sigma)\rangle = \; & \exp(-n\langle\sigma\rangle) \\ & \cdot \exp\left(+\frac{n^2}{2!}\langle(\sigma-\langle\sigma\rangle)^2\rangle\right) \\ & \cdot \exp\left(-\frac{n^3}{3!}\langle(\sigma-\langle\sigma\rangle)^3\rangle\right) \\ & \cdot \exp\left(+\frac{n^4}{4!}[\langle(\sigma-\langle\sigma\rangle)^4\rangle - 3\langle(\sigma-\langle\sigma\rangle)^2\rangle^2]\right) \cdot \ldots ,\end{aligned} \tag{1}$$

where σ is the total cross section. Average brackets, $\langle ... \rangle$, denote averages over energy intervals containing statistically meaningful samples of the fluctuations. Fig. 1 shows that for a fairly thick iron sample the fluctuation (self-shielding) correction factors in Eq. 1 drop below 10 % only above 3 to 4 MeV, whereas the analysed resonance region ends already at 0.86 MeV. The required 2nd, 3rd and 4th moments were directly obtained as sample moments from high-resolution data measured at Geel.

The 2nd moment can, moreover, be predicted from the statistical model of resonance reactions (Hauser-Feshbach theory). [1]: With the conventional definition of the cross sections for compound nucleus formation and for nonelastic processes per entrance channel c,

$$\sigma_c^{CN} = \pi\lambda^2 g_c (1 - |\langle S_{cc}\rangle|^2), \tag{2}$$

$$\sigma_c^{non} = \pi\lambda^2 g_c (1 - \langle |S_{cc}|^2\rangle), \tag{3}$$

(spin factor g_c, S-matrix element S_{cc}) the variance of the total cross section can be written as

$$(\Delta\sigma)^2 = 2\pi\lambda^2 \sum_c g_c(\sigma_c^{CN} - \langle\sigma_c^{non}\rangle). \tag{4}$$

The cross sections encountered here can be computed as usual, σ_c^{CN} from a suitable optical-model potential and $\langle\sigma_c^{non}\rangle$ from average resonance parameters (strength functions) either in many-level Breit-Wigner approximation with width fluctuation corrections (Dresner factors) or, more rigorously, with the GOE triple integral [2]. Relative standard deviations thus computed for iron agree well with empirical values obtained from the high-resolution data (see Fig. 2). It is found again that the fluctuations, and hence self-shilding, are important below 3 or 4 MeV. This conclusion was actually confirmed by recent shielding benchmark calculations at Petten and Frascati, performed with smooth and with fluctuating elastic and inelastic scattering cross sections for iron, with fluctuations taken over directly from the total cross section [3].

[1] F.H. Fröhner, Proc. Int. Conf. on Nucl. Data in Sci. and Technol., Gatlinburg 1994, (J.K. Dickens, ed.), La Grange (1994) vol. 2, p. 597

[2] J.M. Verbaarschot, H.A. Weidenmüller, M.R. Zirnbauer, Phys. Repts. 129 (1985) 367

[3] A. Hogenbirk, ECN Petten, private communication (May 1995)

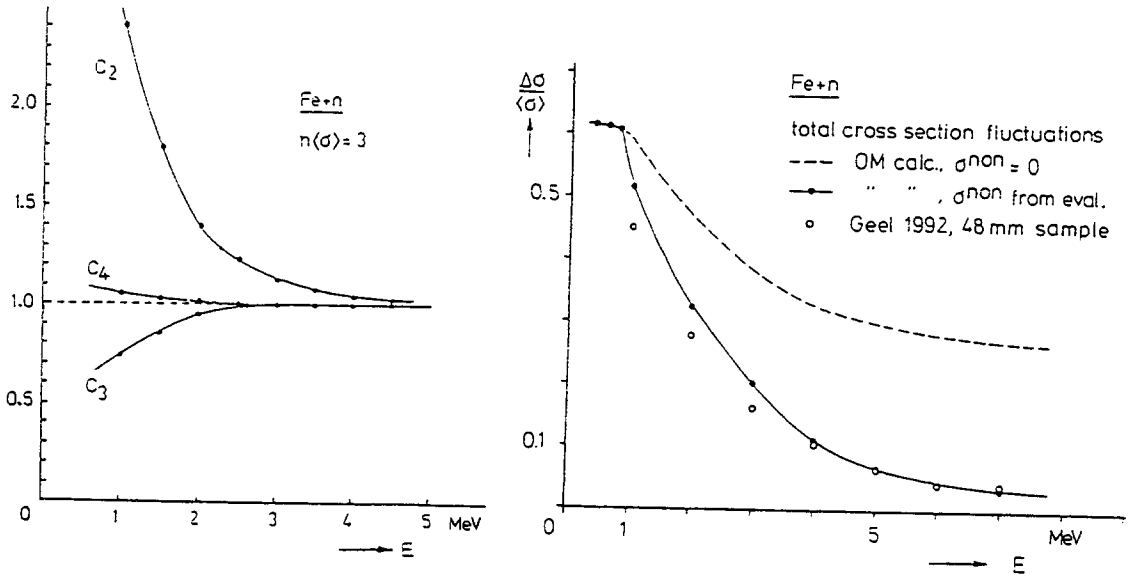

Fig. 1 (left) - First three correction factors in Eq. 1 for an iron sample, effective thickness three mean paths ($n\langle\sigma\rangle = 3$), with moments obtained from Geel data in $\pm$ 10 % energy windows.
Fig. 2 (right) - Calculated and observed relative standard deviations of the total cross section of iron. Difference between dashed and solid curve shows impact of nonelastic reactions.

INSTITUT FÜR NUKLEARCHEMIE
FORSCHUNGSZENTRUM JÜLICH

1. Complex Particle Emission Reactions

S. Merchel, M. Faßbender, B. Scholten, S.M. Qaim, G. Stöcklin

In continuation of our fundamental studies on complex particle emission reactions [cf. 1- 4] the (^{3}He,^{7}Be) process on ^{nat}N, ^{nat}Ne and ^{27}Al was investigated over the ^{3}He-particle energy range of 10 to 36 MeV. The cross sections lie in the mb region and decrease with the increasing mass of the target nucleus. For ^{27}Al, some information on the (p,^{7}Be) and (d,^{7}Be) processes is also available in the literature. A comparison of those data with the present results showed that in the energy region of 15 to 36 MeV the probability of ^{7}Be-emission increases with the increasing mass of the projectile (p<d<^{3}He). A few radiochemical investigations were also performed on the (p,^{7}Be) process on ^{nat}Fe and ^{nat}Cu over the proton energy range of 80 to 180 MeV. Cross sections were measured for the first time and found to be in the range of a few hundred μb.

2. Isomeric Cross Section Ratios

A. Fessler, S.M. Qaim

Continuing our studies on isomeric cross section ratios [cf. 5,6] we investigated the ^{52}Cr(^{3}He,2n)^{53m,g}Fe and ^{52}Cr(^{3}He,3n)^{52m,g}Fe processes from threshold to 35 MeV. For work on the short-lived ^{52m}Fe ($T_{1/2}$ = 46 s) a fast radiochemical separation method was developed. Because of its high spin ($I = 12^{+}$) the ^{52m}Fe was detected so far only in heavy-ion induced reactions. We studied it for the first time in a ^{3}He-particle induced reaction. The results for the two isomeric pairs are shown in Fig. 1. As expected, in both cases the isomeric cross section ratio increases with increasing projectile energy. However, in general the ratio is small even at the highest projectile energy of 35 MeV (0.12 for ^{53m,g}Fe and 0.04 for ^{52m,g}Fe). This is attributed to the high spins of the respective metastable states.

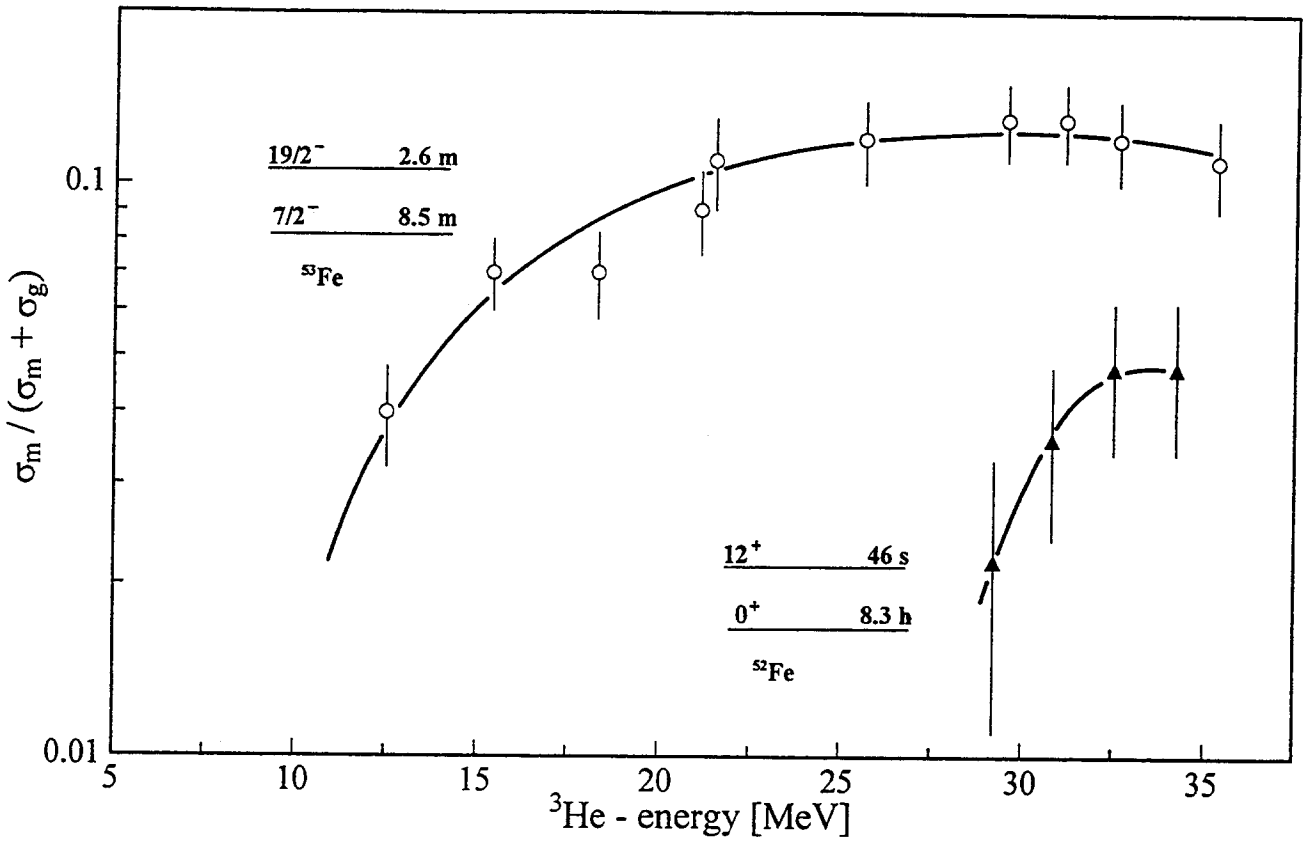

Fig. 1 Isomeric cross section ratios for the isomeric pairs ^{52m,g}Fe and ^{53m,g}Fe produced in (^{3}He,xn) reactions on ^{52}Cr.

3. Fast Neutron Induced Reaction Cross Sections

R. Klopries, R. Dóczi, C. Nesaraja, S.M. Qaim

(Relevant to request identification numbers: 861026 R, 861027 R)

Work on the radiochemical measurement of excitation functions of ^{89}Y(n,2n)^{88}Y, ^{89}Y(n,p)^{89}Sr and ^{89}Y(n,α)^{86}Rb reactions up to 13.3 MeV neutron energy was described in the last Progress Report. The measurement was now extended to the 14 MeV region in collaboration with the Kossuth University, Debrecen, Hungary. The results show smooth trends from the low energy dd neutron data ($E_n \leq 13.3$ MeV) to the higher energy dt data ($E_n \leq 15$ MeV).

Cross sections were measured for the ^{109}Ag(n,2n)^{108m}Ag process at 11 - 12 MeV using highly enriched target material. The reaction product ^{108m}Ag is long-lived ($T_{1/2}$ = 433 y) and rather difficult to characterize. The aim was to check the predictive power of nuclear model calculations. The results are given in Fig. 2. Despite the fact that the investigated product is an isomeric state, the agreement between experiment and theory is good.

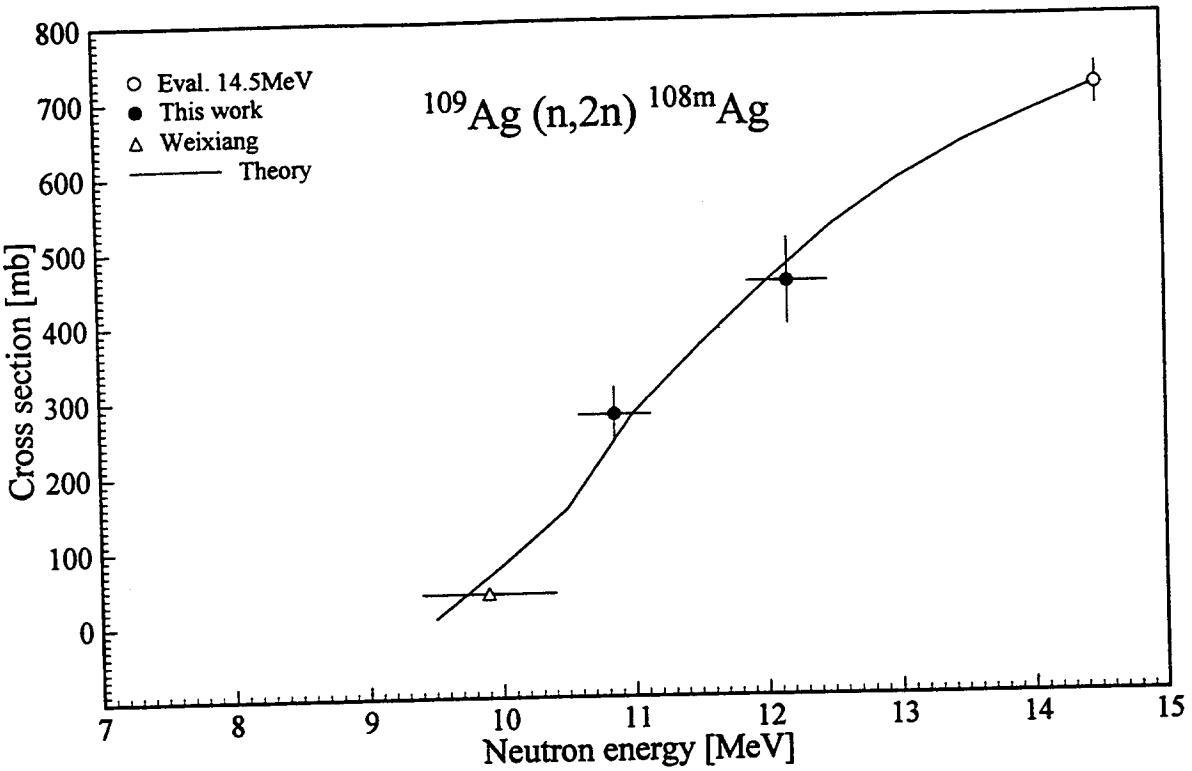

Fig. 2 Excitation function of the $^{109}Ag(n,2n)^{108m}Ag$ process.

The (n,α) reaction cross sections on Ge isotopes are of some interest, both from the fundamental point of view and for estimating radiation damage in semiconductor materials. A study of the $^{72}Ge(n,\alpha)^{69m,g}Zn$ process was initiated and first results in the neutron energy range of 8 to 12 MeV were obtained.

4. Activation Cross Section Data Relevant to Proton Therapy

M. Faßbender, B. Scholten, S.M. Qaim, G. Stöcklin

As mentioned in the last Progress Report, work on measurement of cross sections of nuclear reactions induced by 50 to 250 MeV protons on biologically important materials has been initiated. Of interest are both the short-lived β^+ emitting radio-isotopes (^{11}C, ^{13}N, ^{18}F, etc.) and long-lived activation products (^{7}Be, ^{3}H, ^{22}Na, etc.). In irradiations done at PSI, the excitation functions of $^{nat}C(p,x)^{11}C$ and $^{nat}N(p,x)^{11}C$ processes were determined over the proton energy range of 45 to 70 MeV, the latter for the first time. Regarding the longer-lived activation products, the emphasis was on ^{7}Be-emission cross sections. Irradiations in the 140 to 175 MeV proton energy range were done at Uppsala and the chemical separation and radioactivity measurement at Jülich. Studies on B, C, N, O, Al, Si, Cl, P and S were completed. The measured (p,^{7}Be) excitation functions are relatively flat over the investigated energy range and the trend from the low energy to the higher energy data is quite smooth.

5. Excitation Functions Relevant to Radioisotope Production

F.-O. Denzler, Z. Kovács, F. Tárkányi, R.U. Zaman, B. Scholten, F. Rösch, S.M. Qaim, G. Stöcklin

In continuation of our studies [cf. 7 - 10] on the production of medically important radioisotopes we measured several excitation functions. The emphasis during the present report was on ^{55}Co, ^{124}I and ^{147}Gd.

^{55}Co ($T_{1/2}$ = 17.6 h) is a potentially useful β^+ emitting radioisotope. Of all the processes considered for its production, the $^{58}Ni(p,\alpha)$, $^{56}Fe(p,2n)$ and $^{54}Fe(d,n)$ reactions are very interesting. Whereas the first two reactions have been studied in detail, the information available on the third one was rather scanty. We therefore measured the excitation function of the $^{54}Fe(d,n)^{55}Co$ process using highly enriched ^{54}Fe as target material. Thin target samples were prepared by electrodeposition of ^{54}Fe on Au. The optimum energy range for production of ^{55}Co was found to be E_p = 13 → 3 MeV and the calculated thick target yield amounted to 41 MBq (1.1 mCi)/μAh. The yield is not very high but the process is still promising since it leads to high-purity ^{55}Co.

The radioisotope ^{124}I ($T_{1/2}$ = 4.15 d) is the only longer-lived β^+ emitting isotope of iodine and is used both in diagnostic and therapeutic studies. For its production at a small cyclotron we investigated the $^{124}Te(p,n)^{124}I$ process. Some data were given in the last Progress Report. In cooperation with ATOMKI, Debrecen, Hungary, we now extended those studies up to 31 MeV using a newly developed internal irradiation facility at the Injector Cyclotron of "Cooler Synchroton" (COSY). The energy region E_p = 13 → 9 MeV was found to be optimum for the production of ^{124}I and yields of 20 MBq (0.54 mCi)/μAh can be expected (for more details cf. Ref. [11]).

The γ-ray emitting radioisotope ^{147}Gd ($T_{1/2}$ = 38.1 h) appears to be well-suited for in-vivo pharmakokinetic investigations on the Gd-complexes used as contrast agents in Magnetic Resonance Imaging (MRI). For its production the $^{147}Sm(^3He,3n)$ and $^{144}Sm(\alpha,n)$ reactions appeared to be very promising. We measured the excitation functions of the two processes using highly enriched isotopes as target materials. The results are shown in Fig. 3. In principle both the reactions are suitable for production purposes. In practice, however, the $^{147}Sm(^3He,3n)^{147}Gd$ process was found to be superior since it leads to somewhat higher yields and the cost of the enriched ^{147}Sm is also lower. Over the optimum energy range of $E_{^3He}$ = 36 → 13 MeV the expected thick target yield of ^{147}Gd amounts to 9.5 MBq (0.25 mCi)/μAh and the level of

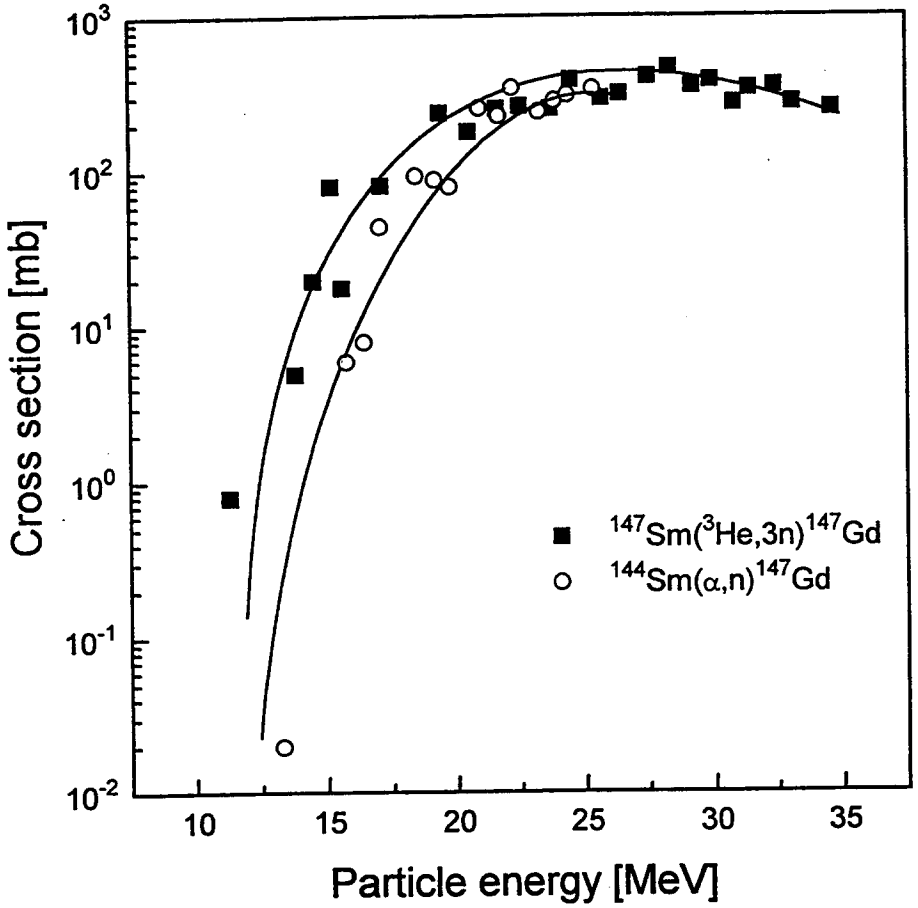

Fig. 3 Excitation functions of nuclear reactions relevant to the production of ^{147}Gd.

^{146,149}Gd isotopic impurities to < 3%. The ^{144}Sm(α,n)^{147}Gd reaction would be more interesting for use at cyclotrons with α ≃ 40 MeV.

References

[1] B. Scholten, S.M. Qaim, G. Stöcklin: Radiochemical studies of proton induced ^{7}Be-emission reactions in the energy range of 40 to 100 MeV, Radiochimica Acta 65 (1994) 81

[2] B. Neumaier, F. Rösch, S.M. Qaim, G. Stöcklin: Radiochemical study of the ^{209}Bi(p,^{7}Be)^{203}Hg-process from 20 to 70 MeV via identification of the emitted particle (^{7}Be) and the product nucleus (^{203}Hg), Radiochimica Acta 65 (1994) 1

[3] S. Sudár, S.M. Qaim: Excitation functions of proton and deuteron induced reactions on iron and alpha-particle induced reactions on manganese in the energy region up to 25 MeV, Phys. Rev. C 50 (1994) 2408

[4] S.M. Qaim, M. Uhl, F. Rösch, F. Szelécsényi: Excitation functions of (p,α) reactions on ^{64}Ni, ^{78}Kr and ^{86}Sr, Phys. Rev. C, in press

[5] S.M. Qaim: Recent developments in the study of isomeric cross sections, Proc. Int. Conf. on Nuclear Data for Science and Technology, Gatlinburg, May 1994, American Nuclear Society (La Grange Park, 1994) p. 186

[6] I.-G. Birn, B. Strohmaier, H. Freiesleben, S.M. Qaim: Isomeric cross section ratios for the formation of ^{75m,g}Ge in (n,p), (n,α) and (n,2n) reactions from 6 to 15 MeV, Phys. Rev. C, in press

[7] A. Fessler, Z.B. Alfassi, S.M. Qaim: Excitation functions of ^{3}He-particle induced nuclear reactions on natural chromium: possibilities of production of ^{52}Fe, ^{53}Fe and ^{52}Mn for medical use, Radiochimica Acta 65 (1994) 207

[8] M. Faßbender, A.F. Novgorodov, F. Rösch, S.M. Qaim: Excitation functions of ^{93}Nb(^{3}He,xn)^{93m,g,94m,g,95m,g}Tc processes from threshold up to 35 MeV: possibility of production of ^{94m}Tc in high radiochemical purity using a thermochromatographic separation technique, Radiochimica Acta 65 (1994) 215

[9] F.-O. Denzler, F. Rösch, S.M. Qaim: Excitation functions of α-particle induced nuclear reactions on highly enriched ^{92}Mo: comparative evaluation of production routes for ^{94m}Tc, Radiochimica Acta 68 (1995) 13

[10] S.M. Qaim, F. Rösch, B. Scholten, G. Stöcklin, Z. Kovács, F. Tárkányi: Nuclear data relevant to the production of the medically important β^+ emitting radioisotopes ^{75}Br, ^{86}Y, ^{94m}Tc and ^{124}I at a small cyclotron, Proc. Int. Conf. on Nuclear Data for Science and Technology, Gatlinburg, May 1994, American Nuclear Society (La Grange Park, 1994) p. 1035

[11] B. Scholten, Z. Kovács, F. Tárkányi, S.M. Qaim: Excitation functions of ^{124}Te(p,xn)^{124,123}I reactions from 6 to 31 MeV with special reference to the production of ^{124}I at a small cyclotron, Appl. Radiat. Isotopes 46 (1995) 255

INSTITUT FÜR KERN-UND TEILCHENPHYSIK
TECHNISCHE UNIVERSITÄT DRESDEN

1. Benchmarks of SS316 Nuclear Data

H. Freiesleben, W. Hansen, D. Richter, K. Seidel, S. Unholzer

1. 1. Introduction

Nuclear shield parameters of fusion reactors such as ITER are determined by the neutron and photon fluxes within and behind the shield. In the development of shield blankets the test of the calculational tools of the neutronics, i.e. nuclear data and codes, has been identified as an important issue [1,2]. Because the structural material of the shield blanket is stainless steel SS316, with iron as the main element, the nuclear data of that material are of exceptionally high importance.
In phase A of shield penetration experiments the total spectral fluences of neutrons and photons from an iron slab (100 x 100 x 30 cm^3) irradiated with 14 MeV neutrons were observed at the position of a point-like detector [3].
In continuation of the programme (Phase B) angular fluences from a SS316 slab were observed for three different directions of the slab.
Because a shield blanket has several ducts and gaps, which effect enhanced radiation load on the coils, also slab assemblies with a gap were investigated. The thickness of the slabs was optimized [4] to be sensitive to both, the nuclear data and streaming through the gap.

1. 2. Geometry and material of the experiment

The geometry of Phase B is shown in Figs. 1 and 2. The collimator was constructed so that only those neutrons and photons leaking from the central part (diameter 12 cm) of the assembly could be observed by the detector. Additionally, the neutron source was positioned in such a way that no directly transmitted but only scattered neutrons move in detector direction. The slab itself had the same dimensions as in Phase A (i.e. a front area of 100 cm x 100 cm and a thickness of 30 cm). A vertical gap with a width of 5 cm was arranged in the centre of the slab.

For a more sensitive investigation of secondary particle angular distributions and of streaming effects the slab was positioned in 3 different orientations to the central collimator axis:

- $\alpha = +24.3°$: gap in direction to the source ("source streaming"), arrangements B10 and B11 without and with gap, respectively,
- $\alpha = 0°$: gap in direction to the detector ("detector streaming"), arrangements B20 and B21 without and with gap, respectively,
- $\alpha = -24.3°$: gap in opposite direction ("diagonal streaming"), arrangements B30 and B31 without and with gap, respectively.

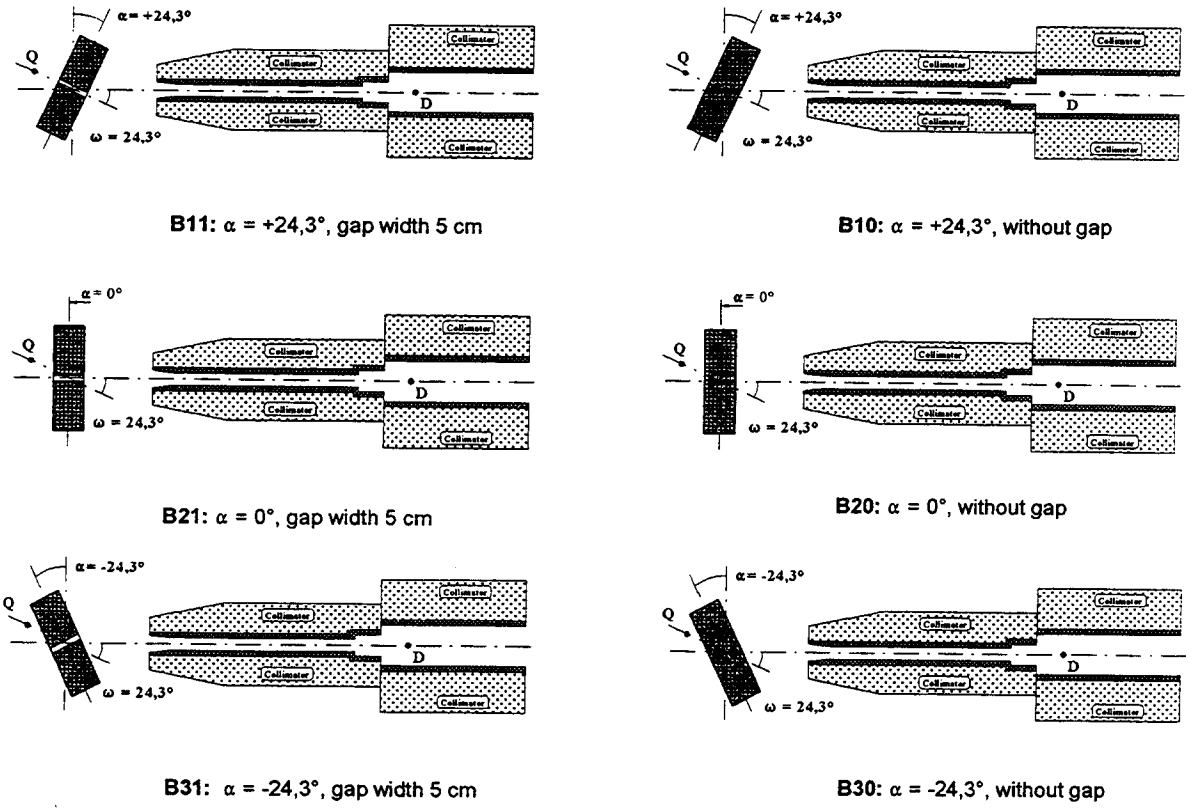

Fig. 1: Geometries investigated (Q: 14 MeV neutron source, D: detector)

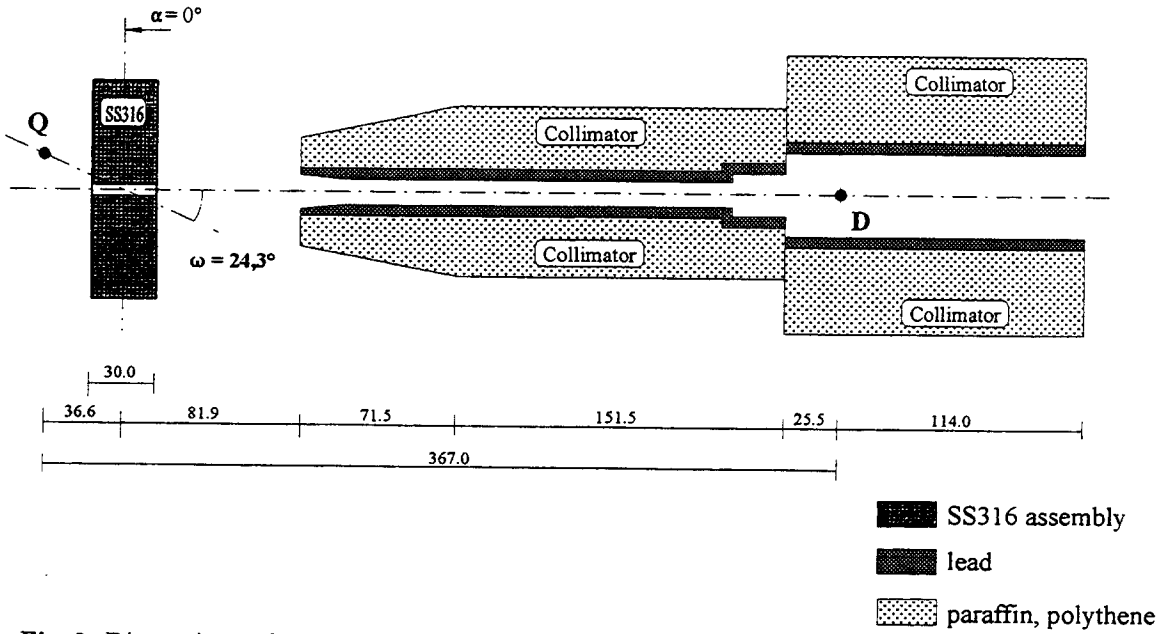

Fig. 2: Dimensions of the experiment (example B21, to scale)
(Q: 14 MeV neutron source, D: detector)

1. 3. Measurements and calculations

A **NE213 scintillator** calibrated at PTB Braunschweig [5-7] was employed for a simultaneous measurement of the spectral neutron flux in the range E > 1 MeV, the spectral photon flux in the range E ≥ 0.2 MeV, and the neutron time-of-arrival spectrum. The pulse height, the time-of-arrival, and a pulse-shape parameter to distinguish between neutrons and photons, were recorded for each registered event.

For the low-energy range of the neutron spectrum a second spectrometer system with **stilbene scintillation detector and hydrogen-filled proportional counters** was employed. The gas filled proportional counters allow the neutron spectra to be measured in the range from about 70 keV (without application of n/γ pulse shape discrimination) to about 1.2 MeV, the stilbene scintillator for E > 700 keV, so that a sufficiently overlapping energy region exists [3].

For the calculations the 3-dimensional Monte-Carlo-code MCNP [8] version 3B, i.e. coupled neutron-photon-transport, was used. As in the experiment the events are acquired two-dimensionally as N(E,t). The data base is EFF-1, the European Fusion File version 1 [9]. Collimator, floor, walls, target backing, air, assembly racks etc. are taken into account, such that the calculated fluences Φ can be compared directly to the measured ones.

1. 4. Results and discussion

The presentation of all spectral distributions would exceed the frame of this report. As a selected but typical example experimental results are shown in Figs. 3 and 4 in comparison to calculated ones for geometry B20 (slab without gap, α = 0°).

All neutron spectra show a surplus of measured neutrons as compared to the calculation for energies of about 3 MeV ... 13 MeV. This tendency is confirmed also in the independently determined $\Phi_n(t)$ for t > 80 ns up to about t = 200 ns.

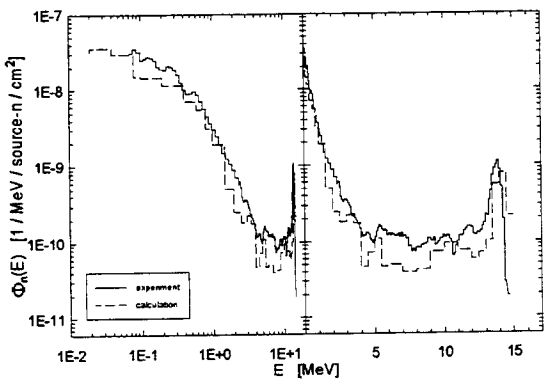

Fig. 3: Spectral neutron fluence for geometry B20 (linear and logarithmic energy axis)

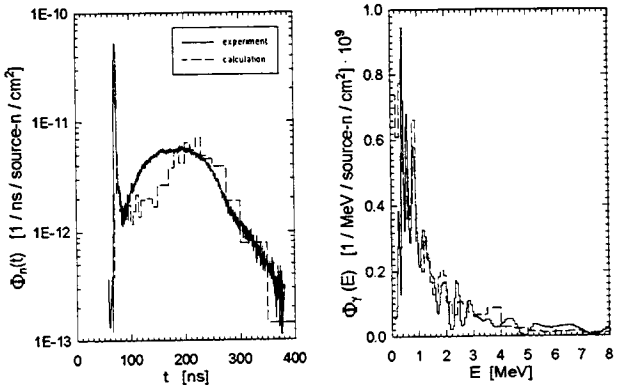

Fig. 4: Neutron time-of-arrival fluence and spectral photon fluence for geometry B20

Similar discrepancies were already stated in the investigations of phase A and discussed in the previous Progress Report [3]. They can be explained in conjunction with the neutron emission cross section, σ_{nm}, at 14 MeV neutron incidence energy. Whereas the angle-integrated energy spectrum of σ_{nm} in EFF-1 is not significantly different from evaluated experimental data and from calculations based on the theory of multistep-direct and multistep-compound mechanisms, differences appear in the angular distributions of the emitted neutrons. Isotropic emission is assumed in the library up to about E = 13 MeV, only the inelastic neutron scattering from the first level of ^{56}Fe (Q = -0.85 MeV) is described anisotropically. However, precompound processes (multistep-direct in the model) are dominating for E > 5 MeV. And these are forward-peaked.

The more forward-oriented neutron transport than described by the library EFF-1 data may also explain the enhanced photon fluence of the experiments. The photons observed originate from a surface region of relatively small thickness facing the detector (for instance 85% of all photons stem from 5 cm thickness), the others from the volume are absorbed. The photon production cross section itself seems to be well described by the library data, also the spectral distribution of photons produced by 14 MeV neutrons agrees with the experimental data.
In the data library EFF-2 the neutron emission is described double-differentially (i.e. energy and angle dependent). As a next step the calculations will be repeated with these data.

As in phase A, a remarkable neutron excess is measured again in the energy range E < 0.2 MeV, i.e. in and below the region of strongly fluctuating resonance cross sections [3]. The underestimation of the neutron fluences at those energies in all assemblies investigated may indicate the need of improved parameters for the resolved and unresolved resonance region.

A gap has remarkable influence on both the neutron and the photon fluence penetrating and leaking the slab assembly. That is demonstrated by the Figs. 5 and 6 for the measured spectral fluences (selected as typical example for geometries B10 and B11 with α = +24.3°). Whereas the low-energy part of the neutron spectra is only weakly influenced by the gap, at energies with forward-peaked neutron emissions a remarkable streaming is observed. With improved neutron data the spectral neutron fluences from the slab assemblies with gap should be re-analyzed in order to separate streaming effects. At present the interference of streaming and inadequate data is strong.

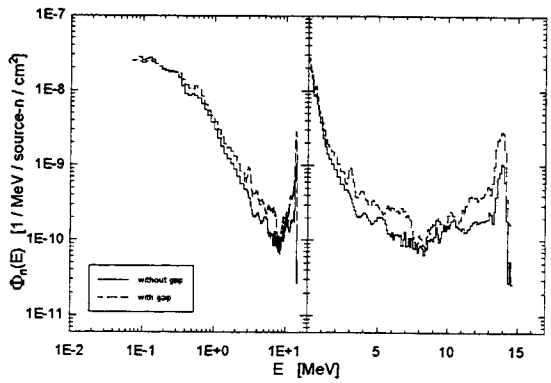

Fig. 5: Influence of the gap on the spectral neutron fluences (experiment), geometries B10 and B11

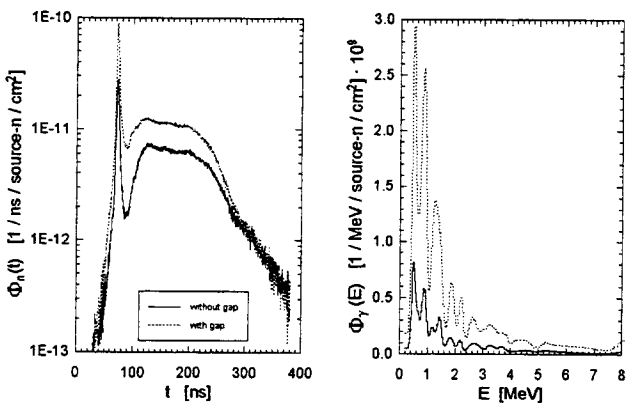

Fig. 6: Influence of the gap on the neutron time-of-arrival fluences and spectral photon fluences (experiments), geometries B10 and B11

References

[1] W. Daenner, ITER Expert Meeting on Shielding Experiments and Analysis, Garching (FRG), Febr. 12-14, 1990, ITER-IL-5-0-5, (1990)

[2] A. Santamarina and T. Parish, Sensitivity and Uncertainty Analysis of the NET Magnet Neutronic Design Parameters to Uncertainties in Cross Section Data, CEA 917/333 (1991)

[3] H. Freiesleben, W. Hansen, D. Richter, K. Seidel, S. Unholzer, Benchmarks of Iron Nuclear Data, Progress Report on Nucl. Data in the FRG, NEA/NSC/DOC(94)21, 1994

[4] T. Elfruth, J. Hanke, K. Seidel and S. Unholzer. Shield penetration experiment. in: Proc. 17th Int. Symp. on Fusion Technology. Rome. 1992. ed. C. Ferro, M. Gasparotto, H. Knoepfel (North-Holland. Amsterdam. 1993) pp. 1341-1345.

[5] S. Guldbakke, H. Klein, A. Meister, J. Pulpan, U. Scheler, M. Tichy, S. Unholzer, Response Matrices of NE213 Scintillation Detectors for Neutrons, Reactor Dosimetry ASTM STP 1228, Ed. H. Farrar et al., American Society for Testing Materials, Philadelphia, 1995, p. 310-322

[6] L. Büermann, S. Ding, S. Guldbakke, S. Klein, H. Novotny, M. Tichy, Response of NE213 Liquid Scintillation Detectors to High-Energy Photons, Nucl. Instr. Methods A 332(1993)483

[7] M. Tichy, The DIFBAS Program - Description and User's Guide, Report PTB-7.2- 193-1, Braunschweig 1993

[8] J. F. Briesmeister. MCNP - A general Monte Carlo code for neutron and photon transport. LA-7396. Los Alamos N. L. (1986).

[9] H. Gruppelaar. Processing of the EFF-1 and EFF-2 data files. EFF-Doc-46.

2. Benchmark Experiment and EFF-2 Iron Nuclear Data

H. Freiesleben, W. Hansen, D. Richter, K. Seidel, S. Unholzer

In previous progress reports measurements of spectral neutron and photon fluxes penetrating and leaking iron slab assemblies irradiated with 14 MeV neutrons were described. The geometry of the assemblies (e.g. Fig. 1) was chosen to be sensitive to employment of nuclear data in the shield blanket design of fusion reactors.

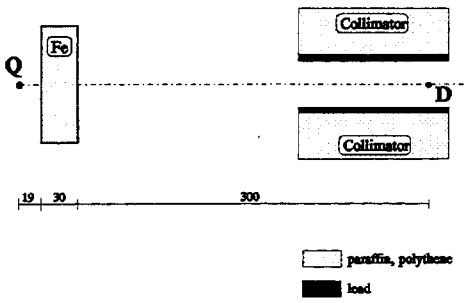

Fig. 1: Horizontal cross section of the benchmark geometry (Q: 14 MeV neutron source; D: detector; Fe: iron slab with dimensions of 100 · 100 · 30 cm³)

The spectral fluxes calculated with the 3-dimensional Monte-Carlo-code MCNP [1] and nuclear data of the European Fusion File version 1 (EFF-1) showed systematic underestimations of the neutron flux in the high-energy region as well as in the corresponding time-of-arrival intervals and of the photon flux in the whole energy range. These discrepancies were discussed [2] in connection with the forward-peaked angular distribution of neutrons inelastically scattered in the pre-compound stage of the interaction, whereas isotropy is assumed for the library data.

In the improved version of the European Fusion File (EFF-2) [3] the neutron emission is described energy-angle differentially [4] and contains forward-peaked components. After availability of a working library [5] for the needed new version of the transport code MCNP-4A [6] the caculations could be carried out with EFF-2. In Fig. 2 measured and calculated spectral neutron fluences from the slab arrangement outlined in Fig. 1 are compared. For 5 MeV < E < 13 MeV a significant improvement with EFF-2 is observed compared to the EFF-1 calculation. The neutron fluence is enhanced by a factor of about 1.4. This is in agreement with results of U. Fischer [7]. The underestimation of the neutron fluence for E < 0.2 MeV, which can not be caused by anisotropy effects, remains.

The time-of-arrival spectrum of the neutrons at the detector position (Fig. 3) shows a similar behaviour. For t > 80 ns (after the peak of penetrating and elastically scattered 14 MeV neutrons) the fluence is significantly enhanced by EFF-2 compared to EFF-1 up to the detector threshold.

The anisotropy of the neutron inelastic scattering has a remarkable influence on the photon fluence too, as shown in Fig. 4. The absorption length of the photons is smaller than the slab thickness. The photons observed origininate from a relatively thin layer facing the detector, and the more forward-oriented neutron transport enhances the photon production in this layer.

An overview of the improvements achieved with the EFF-2 data compared to EFF-1 for shield blanket problems is presented in Tables 1-3.

References

[1] J. F. Briesmeister (Ed.). MCNP - A general Monte Carlo code for neutron and photon transport. LA-7396. Los Alamos. Sep. 1986.

[2] H. Freiesleben, W. Hansen, D. Richter, K. Seidel, S. Unholzer, Experimental Investigation of Neutron and Photon Penetration and Streaming through Iron Assemblies. Fusion Engineering and Design. 1995.

[3] J. Kopecky, H. Gruppelaar and D. Nierop. Status of the European Fusion File. EFF-DOC-242. Dec. 1993.

[4] G. Reffo and M. Hermann. Evaluation of the double-differential neutron spectrum from Fe-56. EFF-DOC-235. June 1993.

[5] L. Petrizzi. Processing EFF-2.3 with ACER and NJOY to procedure an MCNP working library. EFF-DOC-368. Dec. 1994.

[6] J. F. Briesmeister (Editor). MCNP - A General Monte Carlo Code N Particle Transport Code, Version 4A. LA-12625. Los Alamos. Nov. 1993.

[7] U. Fischer, FZ Karlsruhe, INR, private communication

Table 1: Neutron fluence in energy intervals [10^{-9} / cm^2 / source neutron]

E [MeV]	Experiment	Calculation		Calculation / Experiment	
		EFF-1	EFF-2	EFF-1	EFF-2
0.04 - 1.0	317 ± 35	274 ± 4	281 ± 4	0.86	0.89
1.0 - 5.0	45 ± 1	41 ± 1	43 ± 1	0.91	0.96
5.0 - 10.0	3.4 ± 0.1	2.2 ± 0.1	3.2 ± 0.3	0.65	0.94
10.0 - 15.0	15.9 ± 0.3	12.3 ± 0.4	13.9 ± 0.3	0.77	0.87

Table 2: Neutron fluence in time-of-arrival intervals [10^{-9} / cm^2 / source-neutron]

t [ns]	Experiment	Calculation		Calculation / Experiment	
		EFF-1	EFF-2	EFF-1	EFF-2
62 - 81	312 ± 6	255 ± 8	260 ± 1	0.82	0.83
81-200	713 ± 58	537 ± 9	602 ± 4	0.75	0.84

Table 3: Photon fluence in the measured energy range [10^{-10} / cm^2 / source-neutron]

E [MeV]	Experiment	Calculation		Calculation / Experiment	
		EFF-1	EFF-2	EFF-1	EFF-2
0.2 - 8.0	275 ± 4	171 ± 3	219 ± 3	0.62	0.80

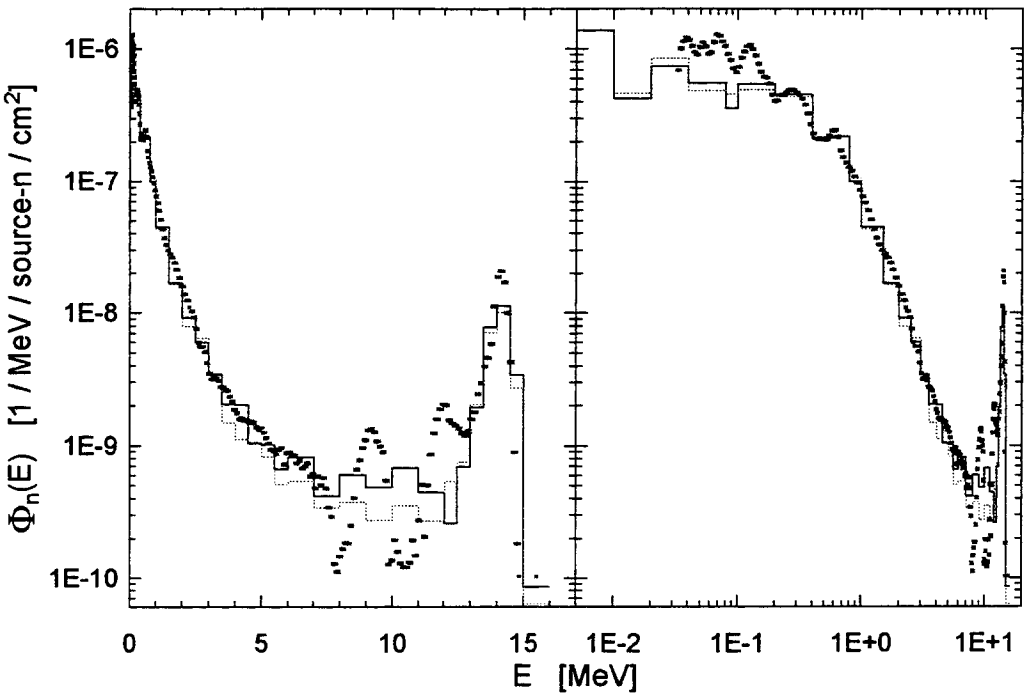

Fig.2: Spectral neutron fluence per one source neutron, measured (*) and calculated with EFF-2 (——) and with EFF-1 (-----)

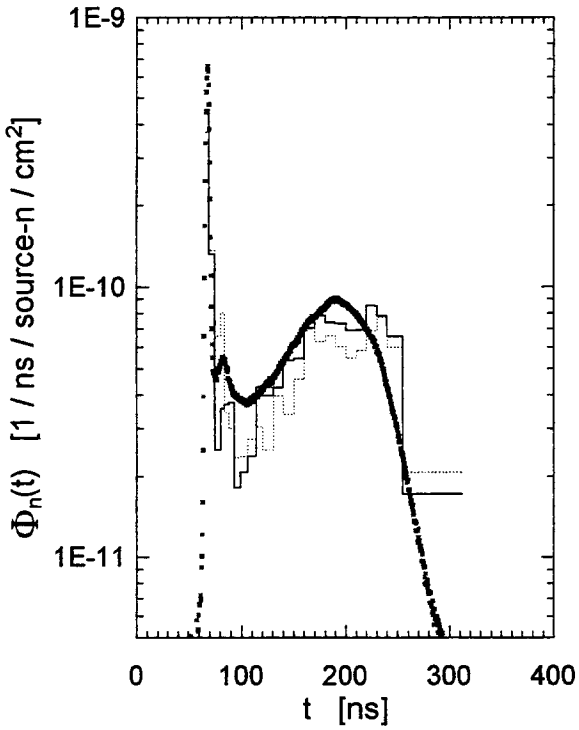

Fig.3: Time-of-arrival spectrum of the neutron fluence per one source neutron, measured (*) and calculated with EFF-2 (——) and with EFF-1 (-----)

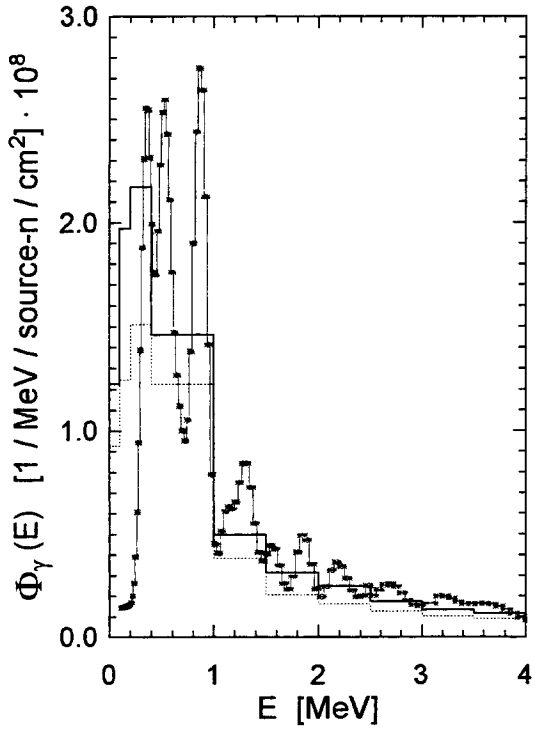

Fig.4: Spectral photon fluence per one source neutron, measured (*) and calculated with EFF-2 (——) and with EFF-1 (-----)

3. X-Ray Line Widths in Elements with Opened 3d Subshells

D.Küchler, U.Lehnert, G.Zschornack

In X-ray fluorescence spectra in the region $20 \leq Z \leq 30$ the K diagram lines often appear too close to each other to allow determination of exact energies, intensities and half widths of the component lines. Thus, there are only a few data, often differing from each other, for the named quantities. Energy differences between the components of the K_α doublet are very small [1]. This is the reason for many difficulties in measuring and deconvoluting the K_α doublet. Thus, only the application of crystal diffraction spectrometers allows to accomplish precise measurements. The obtained data are of some interest for a large field of applications, so for studies of the fine structure of X-ray emission spectra, chemical shifts of X-ray lines and in X-ray photoelectron spectroscopy.

Table 1: Experimental values for natural X-ray line widths of $K_{\alpha_{1,2}}$ doublets. The quantity Γ_A characterizes L_2-L_3X Coster-Kronig transitions, transforming an initial vacancy in the L_2 subshell to the L_3 subshell. The values Γ_A^{th} are theoretical results from Yin et al. [19]. Results for copper are listed for three different assumptions regarding the energies: a: $L_2 - L_3M_4$ and $L_2 - L_3M_5$ transitions are possible; b: $L_2 - L_3M_5$ transitions are possible but $L_2 - L_3M_4$ transitions are not; c: neither $L_2 - L_3M_4$ nor $L_2 - L_3M_5$ transitions are energetically possible.

element	transition	line width/eV	$\Gamma_A(L_2 - L_3X)$/eV	$\Gamma_A^{th}(L_2 - L_3X)$/eV
iron Z = 26	K_{α_1} K_{α_2}	1.85 ± 0.08 2.93 ± 0.09	1.08 ± 0.12	0.583
cobalt Z = 27	K_{α_1} K_{α_2}	2.00 ± 0.06 2.88 ± 0.05	0.88 ± 0.08	
nickel Z = 28	K_{α_1} K_{α_2}	2.25 ± 0.10 3.05 ± 0.08	0.80 ± 0.13	0.801
copper Z = 29	K_{α_1} K_{α_2}	2.53 ± 0.05 2.80 ± 0.08	0.27 ± 0.09	a: 0.922 b: 0.318 c: 0.00476

Without mentioning very early works [2–7] there are only a few papers containing data on X-ray line widths in the above mentioned Z region. Pessa [8] lists K_{α_1} and K_{α_2} natural line widths published in earlier works [2–7] and own measured values. Salem and Lee [9] have determined K X-ray line widths by constructing last-squares fits to the data available in 1976. Semi-empirical values of K_α line widths were published by Krause and Oliver [10]. There the X-ray widths were calculated as the sums of pertinent level widths, whereby level widths were obtained from the relation $\Gamma_i = \Gamma_{R,i}/\omega_i$ with $\Gamma_{R,i}$ as theoretical radiative rates from relativistic, relaxed Hartree-Fock calculations [11, 12] and fluorescence yields from Krause's evaluation [13]. Interpolated widths for Z = 29 are given in Ref.[14]. Blochin and Schweizer [15] tabulate level widths of the $K_{\alpha_{1,2}}$ doublet in the region $22 \leq Z \leq 95$, using values from Refs.[16, 17].

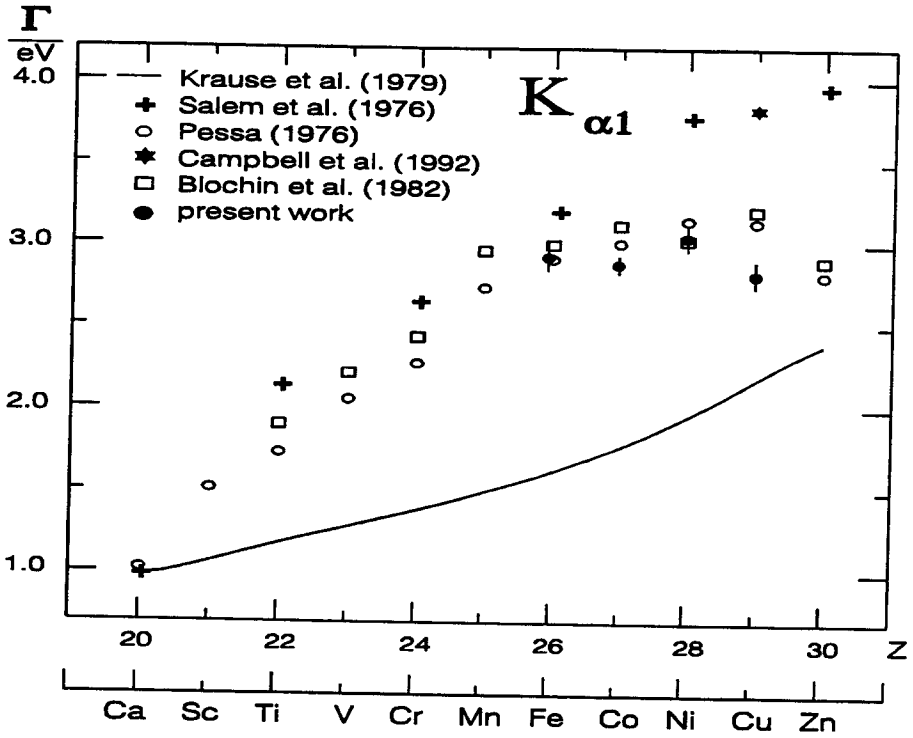

Figure 1: K_{α_1} widths of X-ray lines in the region of 3d elements.

Characteristic X-rays emitted by different X-ray tubes with anode materials Fe, Co, Ni and Cu were analyzed by a high resolving crystal diffraction spectrometer. In our investigations the X-ray tube anode acts as a solid state target. The spectrometer operation scheme is described in Ref.[18]. Both flat crystals as well as focussing ones in Johann geometry were used to measure X-ray spectra from anode materials after electron excitation. For focussing crystals we use only a diaphragm at the front side of the X-ray detector to discriminate the scattered radiation. Using flat crystals a second diaphragm was added. As radiation detector a xenon filled proportional counter was applied.

The results of the spectra processing are summarized in Table 1. As a rule each result was obtained by some measurements of the same line, i.e. values given in Table 1 are mean values with mean errors. The systematic error was estimated by considering the accuracy of the angular positioning of the spectrometer ($\approx 3''$), weighted by the number of channels for each peak flange.

Graphical representations of our results are shown in Figs.1 and 2. Here the often cited semi-empirical values from Krause and Oliver [10] (solid lines) are compared with the values of Salem and Lee [9], Pessa [8], Cambpell and Wang [14] and those of Blochin and Schweizer [15].

In the region of 3d elements a change of the peripheral electron configuration by multiple ionization or by chemical bonding may change level energies and may open or close Coster-Kronig decay channels. For such cases the effect on natural level width is usually dramatic as it is known for example for the L_2-L_3X Coster-Kronig transition [19]. Generally, in contrast to shake-off satellites Coster-Kronig satellites appear on the high energy side of the diagram lines.

Our results confirm in the case of the K_{α_2} line the significant deviations between the results of Krause and Oliver and experimental data. As we see especially in the case of the K_{α_1}, some other authors get results with increased widths in comparison to our results. Possibly

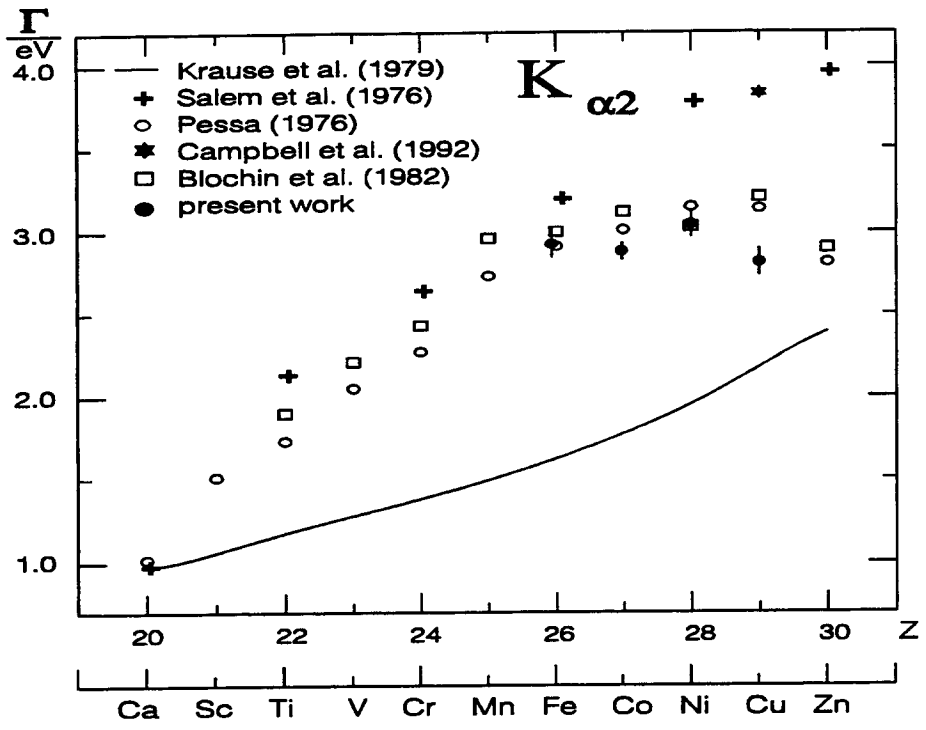

Figure 2: K_{α_2} widths of X-ray lines in the region of 3d elements.

the broadened values result from the deconvolution of asymmetric lines with a symmetric Lorentzian. Our more sensitive deconvolution method (see Ref.[20]) avoids this problem and leads to realistic results.

As shown in Table 1 , from the difference between the K_{α_1} and K_{α_2} level widths the corresponding width for the main Coster-Kronig process can be deduced. In the Coster-Kronig processes a primary vacancy can be shifted from a lower to a higher subshell before it is filled by an electron from another major shell. The derived values of $\Gamma_A(L_2 - L_3X)$ could be compared with theoretical values from the calculation of Yin et al. [19] performed with numerical single-particle wave functions based on Green's atomic independent-particle model [21]. Thereby, the computed radiationless transition probabilities were combined with X-ray emission rates by Scofield [22] to derive total level widths and Coster-Kronig transition probabilities.

In the case of nickel there is an excellent agreement between our value and that of Yin et al. [19], but for iron our result is higher than that of Yin et al. This is pressumably due to somewhat higher than expected width of the iron K_{α_2} transition, whose value we could not explain in the course of our evaluation (see also Fig.2). In contrast to Yin et al. we deduce, that in the case of copper the assumption should be true, that $L_2 - L_3M_5$ Coster-Kronig transitions are possible but $L_2 - L_3M_4$ ones are not.

The used method is applicable to a wide range of elements and for different X-ray series. Thus, we will continue these investigations measuring X-ray fluorescence after electron impact excitation of various probes. This increases significantly the element range for our investigation according to materials available as cathodes in X-ray tubes.

The work has been supported by BMFB under contract No. 06 DD 111 and by Sächsisches Staatsministerium für Wissenschaft und Kunst under contract No. 7541.83-FZR/320.

References

[1] G.Zschornack; Atomdaten für die Röntgenspektralanalyse, Springer-Verlag, Berlin, Heidelberg a.o., 1989

[2] G.Brogren; Arkiv Fysik, 23 (1962) 219

[3] L.G.Parratt; Physical Review, 50 (1936) 1

[4] J.A.Bearden, C.H.Shaw; Physical Review, 48 (1935) 18

[5] A.Meisel, W.Nefedow; Z. Phys. Chem., 219 (1962) 194

[6] L.Obert, J.A.Bearden; Physical Review, 54 (1938) 1000

[7] M.A.Blochin, I.Y.Nikiforov; Bullet. Acad. Sci. USSR, 28 (1964) 689

[8] V.M.Pessa; X-Ray Spectrometry, 2 (1973) 169

[9] S.I.Salem, P.L.Lee; Atomic Data and Nuclear Data Tables, 18 (1976) 223

[10] M.O.Krause, J.H.Oliver; J. Phys. Chem. Ref. Data, 8 (1979) 329

[11] J.H.Scofield; Physical Review, A9 (1974) 1041

[12] J.H.Scofield; Physical Review, A10 (1974) 1507

[13] M.O.Krause; J. Phys. Chem. Ref. Data, 8 (1979) 307

[14] J.L.Camppell, J.X.Wang; X-Ray Spectrometry, 21 (1992) 223

[15] M.A.Blochin, I.G.Schweizer; X-Ray Reference Book (in russian), Nauka, Moscow, 1982

[16] M.A.Blochin; X-Ray Physics (in russian), Gostechizdat, Moscow, 1959

[17] G.C.Nelson, B.G.Saunders; J. de Physique, C4 (1971) 97

[18] U.Lehnert, K.Merla, G.Zschornack; Nucl. Instr. Methods, B89 (1994) 238

[19] L.I.Yin, I.Adler, M.H.Chen, B.Crasemann; Physical Review, A7 (1973) 897

[20] D. Küchler; Diploma Thesis, TU Dresden, FB Physik, 1994.

[21] A.E.S.Green, D.L.Sellin, A.S.Zachor; Physical Review, 184 (1969) 1

[22] J.H.Scofield; Physical Review, 179 (1969) 9

ABTEILUNG NUKLEARCHEMIE
UNIVERSITÄT ZU KÖLN
AND
ZENTRUM FÜR STRAHLENSCHUTZ UND RADIOÖKOLOGIE
UNIVERSITÄT HANNOVER

1. Production of Radionuclides from Target Elements ($22 \leq Z \leq 29$) by Proton-Induced Reactions up to 100 MeV

R. Bodemann[1], R. Michel[2], R. Rösel[2], U. Herpers[2], B. Holmqvist[3], H. Conde[4], P. Malmborg[5]

In the course of a project to measure cosmochemically relevant thin-target cross sections for proton-induced reactions [1-3, and references therein], irradiation experiments were performed at the cyclotron of The Svedberg Laboratory (TSL) of the University of Uppsala. In a first series of exeriments we investigated proton-induced reactions on 18 target elements ($6 \leq Z \leq 56$) up to 100 MeV. The results obtained for the target elements C, N, O, Mg, Al, and Si have already been reported elsewhere [3]. In these experiments we included also target elements such as Ti, V, Mn, Fe, Co, and Ni which were formerly investigated in detail by our group [4, 5]. This was done on the one hand for the purpose of cross checking our procedures and, on the other, and even more importantly, we produced new irradiated targets for destructive analysis by accelerator and classical rare gas mass spectrometry. Here we report the results of the γ-spectrometric analysis of these targets. We also included the target element Cu in these experiments. Copper has been extensively investigated recently [6] and is one of the important target elements used for monitoring purposes. Therefore, a comparison of our results which are based on

1 Zentrum für Strahlenschutz und Radioökologie, Universität Hannover, F.R.G.
2 Abteilung Nuklearchemie, Universität zu Köln, F.R.G.
3 The Studsvik Neutron Research Laboratory, University of Uppsala, Sweden
4 Department of Neutron Research, University of Uppsala, Sweden
5 The Svedberg Laboratory, University of Uppsala, Sweden

aluminum as the monitoring element is of particular interest.

The stacked-foil technique was used in these experiments. The γ-ray spectrometric methods were identical to those used earlier [3-5]. The proton energy in each individual target foil was calculated according to the work of Andersen and Ziegler [7]. The beam current was monitored by the reaction $^{27}Al(p,3p3n)^{22}Na$ using the recommended cross sections from the evaluation by Tobailem and de Lassus St. Genies [8]. As discussed by Bodemann et al. [3] in detail, the proton flux densities were determined for each stack in the first aluminum foil of the entire stack. Therefore, all the results are normalized to the cross sections assumed for the reaction $^{27}Al(p,3p3n)^{22}Na$ at the primary energies used, which were 94.4 MeV and 98.9 MeV, respectively. As discussed in section 2, for these proton energies the excitation function recommended by Tobailem and de Lassus St. Genies [8] for the reaction $^{27}Al(p,3p3n)^{22}Na$ and those recently measured by Steyn et al. [9] are in good agreement. Therefore, our results of the 94.4 MeV and 98.8 MeV irradiations at TSL are not affected by the discrepancies in this monitor reaction discussed in section 2.

In table 1 we report results on 61 individual target/product combinations for the target elements Ti, V, Mn, Fe, Co, Ni, and Cu. Between 2 and 7 energy points were investigated for each reaction. The errors quoted for the cross sections consider all kown sources of errors as discussed in detail in our earlier work [3]. The agreement with our earlier work [4,5] on target elements from Ti to Ni and with that of Mills et al. [6] for Cu is generally excellent.

The situation for cosmochemically target elements ($6 \leq Z \leq 28$) and for the target element Cu is now quite satisfying. The experiments at TSL, which presently are extended to higher proton-energies up to 180 MeV, together with experiments at PSI/Villigen (up to 72 MeV), at CERN (600 MeV), at LANL (800 MeV) and at LNS/Saclay (200 MeV to 2.6 GeV) yielded fairly complete excitation functions for the production of short- and medium-lived γ-emitting radionuclides [10, 11]. Only few gaps have to be closed. The measurements of long-lived radionuclides by accelerator mass spectrometry (AMS) and of stable rare gas isotopes by conventional mass spectrometry will, however, still take considerable time. Also the cosmochemically relevant medium-mass target elements, Zr, Nb, and Ba, which were also part of these experiments, are now completely analyzed with respect to radionuclides and will be published in due course.

In the continuation of our experiments at TSL the target element coverage will be enlarged (40 elements $6 \leq Z \leq 83$) in order to satisfy not only the data

needs of cosmophysical applications but also those of technological applications, such as accelerator based waste transmutation and energy amplification.

2. New Measurements of the Monitor Reactions $^{27}Al(p,X)^{7}Be$, $^{27}Al(p,3p3n)^{22}Na$, $^{27}Al(p,3pn)^{24}Na$ and $^{65}Cu(p,n)^{65}Zn$

R. Bodemann[1], H. Busemann[1], M. Gloris[1], I. Leya[1], R. Michel[2], T. Schiekel[2], U. Herpers[2], B. Holmqvist[3], H. Conde[4], P. Malmborg[5], B. Dittrich-Hannen[6], M. Suter[6]

The necessity to use a multitude of accelerators when investigating nuclide production from thresholds up to 2.6 GeV and the fact that rarely there are possibilites at the different accelerators to determine the absolute flux densities in the targets by reliable Faraday cup measurements make the question of monitor cross sections a crucial one. Moreover, since there are no monitor cross sections which can be used over the entire energy range from 10 or 20 MeV up to 2.6 GeV, the problem is even worse.

Important monitor elements are aluminum and copper. For aluminum, there exist recommended cross sections from the evaluation by Tobailem and de Lassus St. Genies [8] for the reactions $^{27}Al(p,X)^{7}Be$, $^{27}Al(p,3p3n)^{22}Na$, and $^{27}Al(p,3pn)^{24}Na$. Among them, $^{27}Al(p,3p3n)^{22}Na$ has the best experimental data base. Therfore, we used this reaction with the cross sections recommended by Tobailem and de Lassus St. Genies [8] in our determinations of thin-target cross sections of cosmochemically relevant reactions [3-5, 10, 11, and references therein]. We also reported own results of absolute measurements for this reaction [12]. Recently, new absolute measurements for energies up to

1 Zentrum für Strahlenschutz und Radioökologie, Universität Hannover, F.R.G.
2 Abteilung Nuklearchemie, Universität zu Köln, F.R.G.
3 The Studsvik Neutron Research Laboratory, University of Uppsala, Sweden
4 Department of Neutron Research, University of Uppsala, Sweden
5 The Svedberg Laboratory, University of Uppsala, Sweden
6 Inst. für Teilchenphysik, ETH-Hönggerberg, Zürich, Switzerland

200 MeV were reported by Steyn et al. [9]. Their measurements show some significant deviations from the recommendations of Tobailem and de Lassus St. Genies [8] (Fig. 1).

The two excitation functions agree within the limits of the experimental errors given by Steyn et al. [9], but there remain some systematic differences. The data are in excellent agreement from threshold up to 60 MeV. Above 60 MeV the data of Steyn et al. [9] are systematically lower than those recommended by Tobailem and de Lassus St. Genies [8]. Both data sets agree again at 90 MeV. Above 90 MeV up to 200 MeV the data by Steyn et al. [9] are slightly higher than the other ones [8]. At 200 MeV both data sets again agree. Our new experiments at PSI/Villigen (45 MeV and 72 MeV) and at TSL/Uppsala (130 MeV and 180 MeV), in which a large number of aluminum targets were included enabled us to investigate the consistency of the excitation function of this monitor reaction. The results of this investigation are presented in table 2. Our new data for the reaction $^{27}Al(p,3p3n)^{22}Na$ together with our earlier results [12] support the excitation function obtained by Steyn et al. [9], which will be used furtheron by us for monitoring.

Simultaneous investigations of targets irradiated at PSI/Villigen, TSL/Uppsala and LNS/Saclay enabled us to present new comprehensive data for the reactions $^{27}Al(p,X)^{7}Be$ and $^{27}Al(p,3pn)^{24}Na$, for which the data base was less complete and partially contradictory up to now. The new data are presented in table 3 for $^{27}Al(p,X)^{7}Be$ and in table 4 for $^{27}Al(p,3pn)^{24}Na$. For the latter reaction, there exist additional measurements from our group [5] which are not included in table 4. Thus, we now have a consistent set of excitation functions from thresholds up to 2.6 GeV for the three monitor reactions $^{27}Al(p,X)^{7}Be$, $^{27}Al(p,3p3n)^{22}Na$, and $^{27}Al(p,3pn)^{24}Na$.

When going to proton-energies below 50 MeV, aluminum is not well suited as a monitoring target element, because one has to measure near the threshold where the energy determination becomes crucial. Here, copper offers an alternative solution. The reaction $^{65}Cu(p,n)^{65}Zn$ is applicable down to energies of less than 10 MeV. For this reaction also recent absolute measurements by Mills et al. [6] exist. We have determined the excitation function of this reaction relative to the aluminum monitoring reactions. The results of our investigation (table 5) are in excellent agreement with those reported by Mills et al. [6]. Our measurements describe the reaction up to 375 MeV. At higher energies, (p,n)-reactions are not suitable as monitor reactions because they become extremely sensitive to interferences by low-energy secondary protons and

secondary light complex particles [10].

3. Production of ^{36}Cl from Calcium, Titanium, Manganese, Iron, Cobalt and Nickel by Proton-Induced Reactions

T. Schiekel[1], F. Sudbrock[1], U. Herpers[1], I. Leya[2], R. Michel[2], H.-A. Synal[3], M. Suter[3]

Integral excitation functions for the production of cosmogenic nuclides are of fundamental importance for the interpretation of the interactions of solar and galactic cosmic ray particles with terrestrial and extraterrestrial matter [1]. In continuation of our long-term efforts to measure cosmochemically relevant excitation functions for the production of long-lived radionuclides [2] we investigated the production of ^{36}Cl from natural Ca, Ti, Mn, Fe, Co and Ni.

We analyzed targets from irradiations with protons of energies between 45 MeV and 2.6 GeV at several accelerators (PSI-Villigen/CH, TSL-Uppsala/S, LNS-Saclay/F). The experiments were carried out using the stacked-foil technique at PSI and TSL. At LNS small stacks were irradiated providing just one energy point per irradiation. Experimental techniques, data evaluation and flux monitoring were identical to those reported earlier [3-5, 10, 11]. Details of the chemical separations for the extraction of ^{36}Cl (and other long-lived radionuclides) from the targets may be found elsewhere [14]. ^{36}Cl together with about 5 mg stable carrier was converted to AgCl. The samples were measured by accelerator mass spectrometry at the PSI/ETH Tandem AMS Facility at the ETH Hönggerberg-Zürich/CH . For the investigations the standard "K380/4" was used which has a $^{36}Cl/^{nat}Cl$ ratio of $(1.53 \pm 0.15) * 10^{-11}$ [15]. The results obtained up to now are presented in table 6. The investigations will be continued to complete the excitation functions from thresholds up to 2.6 GeV. The new data will be used for modelling the production of ^{36}Cl in meteoroids and lunar surface samples as soon as they are validated by model calculations for

1 Abteilung Nuklearchemie, Universität zu Köln, F.R.G.
2 Zentrum für Strahlenschutz und Radioökologie, Universität Hannover, F.R.G.
3 Inst. für Teilchenphysik, ETH-Hönggerberg, Zürich, Switzerland

^{36}Cl in simulation experiments in which artificial meteoroids were irradiated isotropically by 1.6 GeV protons.

Acknowledgement The authors thank the authorities of the Laboratoire National Saturne/Saclay, of the Paul Scherrer Institute/Villigen and of The Svedberg Laboratory/University of Uppsala for the beam-time and the accelerator for their cooperation. This work was suported by the Deutsche Forschungsgemeinschaft.

References

[1] R. Michel, in: Intermediate Energy Nuclear Data for Applications, N.P. Kocherov (ed.), INDC(NDS)-245, IAEA, Vienna, (1991), p. 17

[2] R. Michel, Nuclear Data for the Interpretation of Cosmic Ray Interactions with Matter, Proceedings Int. Conf. Nuclear Data for Science and Technology, May 9-13, 1994, Gatlinburg, Tennessee, USA, J.K. Dickens (ed.), pp. 337 - 343 (1994) American Nuclear Society, Inc., La Grange Park, Illinois

[3] R. Bodemann, H.-J. Lange, R. Michel, T. Schiekel, R. Rösel, U. Herpers, H.J. Hofmann, B. Dittrich, M. Suter, W. Wölfli, B. Holmqvist, H. Condé, P. Malmborg, Nucl. Instr. Meth. Phys. Res. B82 (1993) 9

[4] R. Michel and R. Stück, Proc. 14th Lun. Plan. Sci. Conf., J. Geophys. Res. 89 (1984) B673

[5] R. Michel, F. Peiffer and R. Stück, Nucl. Phys. A 441 (1985) 617

[6] S.J. Mills, G.F. Steyn, F.M. Nortier, Appl. Radiat. Isot. 43 (1992) 1019

[7] H.H. Andersen and J.F. Ziegler, Hydrogen Stopping Powers in All Elements, Pergamon Press (1977)

[8] J. Tobailem and C.H. de Lassus St. Genies, CEA-N-1466(5) (1981)

[9] G.F. Steyn, S.J. Mills, F.M. Nortier, B.R.S. Simpson, B.R. Meyer, Appl. Radiat. Isot. 41 (1990) 315

[10] R. Michel, M. Gloris, H.-J. Lange, I. Leya, M. Lüpke, U. Herpers, B. Dittrich-Hannen, R. Rösel, Th. Schiekel, D. Filges, P. Dragovitsch, M.Suter, H.-J. Hofmann, W. Wölfli, P.W. Kubik, H. Baur, R. Wieler, submitted to Nucl. Instr. Meth. Phys. Res. B (1995)

[11] Th. Schiekel, F. Sudbrock, U. Herpers, M. Gloris, H.-J. Lange, I. Leya, R. Michel, B. Dittrich-Hannen, H.-A. Synal, M. Suter, P.W. Kubik, D. Filges, to be submitted to Nucl. Instr. Meth. Phys. Res. B (1995)

[12] R. Michel, G. Brinkmann and W. Herr, in: Progress Report on Nuclear Data Research in Germany, S.M. Qaim (ed.), NEANDC(E)-202 U Vol. V INDC(GER)-21/L + Special (1979) p.68

[13] Th. Schiekel, R. Rösel, U. Herpers, I. Leya, M. Gloris, R. Michel, B. Dittrich-Hannen, P.W. Kubik, H.-A. Synal, M. Suter, Cross sections for the p-induced production of longlived radionuclides for the interpretation of cosmogenic nuclides, Proceedings Int. Conf. Nuclear Data for Science and Technology, May 9-13, 1994, Gatlinburg, Tennessee, USA, J.K. Dickens (ed.), pp. 344 - 346 (1994) American Nuclear Society, Inc., La Grange Park, Illinois

[14] Th. Schiekel, Thesis, University of Cologne, 1995

[15] H.-A. Synal, Thesis, ETH-Zürich, ETH-8987, 1989

[16] Th. Schiekel, U. Herpers, R. Michel, H.-A. Synal, M. Suter, On the Production of ^{36}Cl in Extraterrestrial Matter, PSI Annual Report 1995, in press

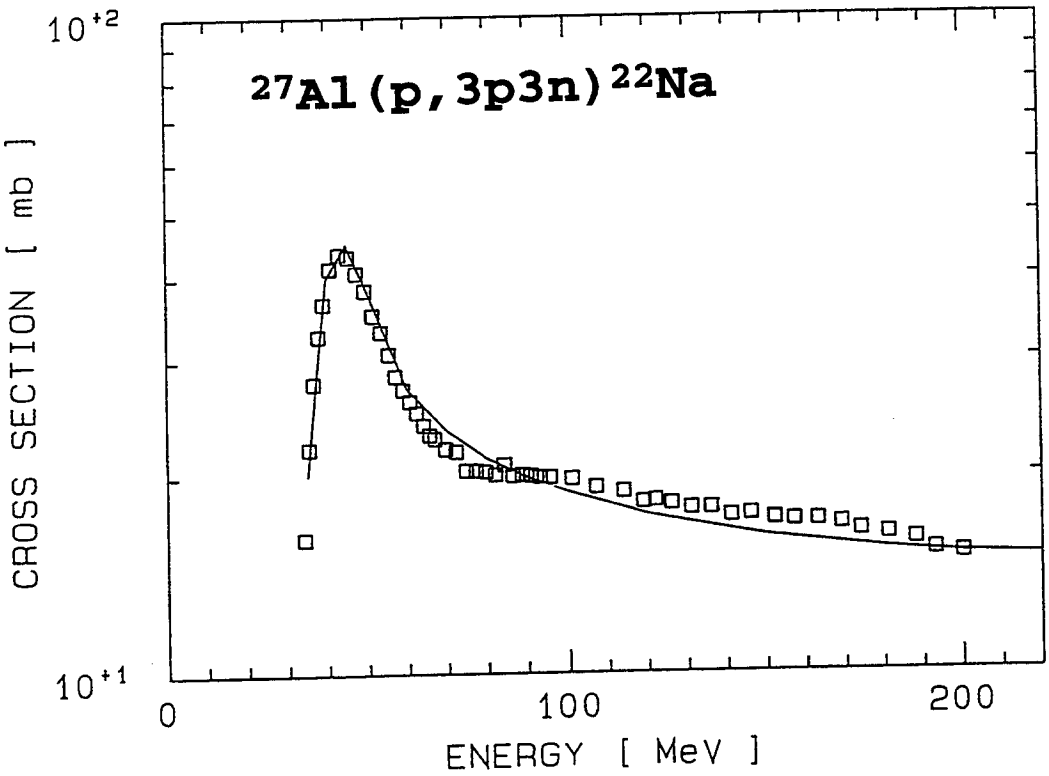

Fig. 1: Excitation function for the production of ^{22}Na from proton irradiation of aluminum as recommended by Tobailem et al. [8] (full line) and as measured recently by Steyn et al. [9] (open squares).

Table 1: Cross sections [mb] for proton-induced reactions on Ti, V, Mn, Fe, Co, Ni, and Cu measured by γ-ray spectrometry. All cross sections are cumulative, except for those marked by "(i)" after the reaction as independent ones.

ENERGY [MeV]	CROSS SECTION [mb]
Ti(p,3pXn)^{47}Ca	
66.9 ± 1.0	0.046 ± 0.012
82.0 ± 0.7	0.071 ± 0.013
95.3 ± 0.5	0.075 ± 0.014
Ti(p,2pXn)^{44m}Sc (i)	
28.9 ± 2.6	14.0 ± 1.5
48.8 ± 1.5	11.7 ± 1.2
66.9 ± 1.0	19.6 ± 2.1
82.0 ± 0.7	20.6 ± 2.2
95.3 ± 0.5	18.1 ± 1.9
Ti(p,2pXn)^{46}Sc (i)	
28.9 ± 2.6	13.0 ± 1.3
48.8 ± 1.5	60.9 ± 6.2
60.3 ± 1.3	54.3 ± 5.6
66.9 ± 1.0	46.4 ± 4.7
82.0 ± 0.7	43.3 ± 4.4
92.0 ± 0.6	44.2 ± 4.6
95.3 ± 0.5	40.1 ± 4.1
Ti(p,2pXn)^{47}Sc	
28.9 ± 2.6	20.4 ± 2.1
48.8 ± 1.5	19.5 ± 2.0
66.9 ± 1.0	19.6 ± 2.0
82.0 ± 0.7	19.6 ± 2.0
95.3 ± 0.5	19.2 ± 2.0
Ti(p,2pXn)^{48}Sc (i)	
48.8 ± 1.5	1.67 ± 0.23
66.9 ± 1.0	1.82 ± 0.23
82.0 ± 0.7	1.87 ± 0.25
95.3 ± 0.5	2.01 ± 0.26
Ti(p,Xn)^{48}V (i)	
28.9 ± 2.6	36.9 ± 3.7
48.8 ± 1.5	17.4 ± 1.8
60.1 ± 0.9	13.6 ± 1.4
66.9 ± 1.0	11.1 ± 1.1
82.0 ± 0.7	8.52 ± 0.86
92.0 ± 0.6	7.53 ± 0.81
95.3 ± 0.5	6.88 ± 0.70
V(p,3pXn)^{46}Sc (i)	
59.8 ± 0.8	20.2 ± 2.1
91.7 ± 0.4	24.7 ± 2.6
V(p,pXn)^{48}V	
59.8 ± 0.8	99.8 ± 10.4
91.7 ± 0.4	51.7 ± 5.4

ENERGY [MeV]	CROSS SECTION [mb]
V(p,Xn)^{51}Cr (i)	
59.8 ± 0.8	14.4 ± 1.7
91.7 ± 0.4	8.68 ± 1.07
Mn(p,5p7n)^{44m}Sc (i)	
81.2 ± 0.9	0.472 ± 0.087
81.2 ± 0.9	0.443 ± 0.234
94.6 ± 0.6	1.38 ± 0.14
94.6 ± 0.6	1.64 ± 0.33
Mn(p,5p5n)^{46}Sc (i)	
59.4 ± 1.0	2.22 ± 0.18
66.0 ± 1.2	3.01 ± 0.23
81.2 ± 0.9	2.22 ± 0.18
91.3 ± 0.5	2.75 ± 0.23
94.6 ± 0.6	2.97 ± 0.23
Mn(p,5p4n)^{47}Sc	
47.7 ± 1.7	0.321 ± 0.061
66.0 ± 1.2	0.300 ± 0.041
81.2 ± 0.9	0.677 ± 0.076
94.6 ± 0.6	1.82 ± 0.19
Mn(p,3p5n)^{48}V	
59.4 ± 1.0	4.41 ± 0.39
66.0 ± 1.2	13.7 ± 1.0
81.2 ± 0.9	20.2 ± 1.5
91.3 ± 0.5	19.1 ± 1.5
94.6 ± 0.6	16.4 ± 1.2
Mn(p,2p3n)^{51}Cr	
27.8 ± 2.9	77.3 ± 5.8
47.7 ± 1.7	16.3 ± 1.3
59.4 ± 1.0	77.7 ± 6.1
66.0 ± 1.2	103. ± 8.
81.2 ± 0.9	96.9 ± 7.5
91.3 ± 0.5	95.3 ± 7.6
94.6 ± 0.6	83.9 ± 6.4
Mn(p,p3n)^{52}Mn	
27.8 ± 2.9	0.189 ± 0.016
47.7 ± 1.7	54.6 ± 4.1
66.0 ± 1.2	40.9 ± 3.1
81.2 ± 0.9	27.5 ± 2.1
94.6 ± 0.6	22.8 ± 1.7
Mn(p,pn)^{54}Mn (i)	
27.8 ± 2.9	414. ± 31.
47.7 ± 1.7	177. ± 13.
59.4 ± 1.0	172. ± 14.
66.0 ± 1.2	147. ± 11.
81.2 ± 0.9	125. ± 10.

ENERGY [MeV]	CROSS SECTION [mb]
Mn(p,pn)^{54}Mn (i)	
91.3 ± 0.5	121. ± 10.
94.6 ± 0.6	109. ± 8.
Fe(p,6pXn)^{44m}Sc (i)	
64.5 ± 1.3	0.117 ± 0.028
79.8 ± 0.9	0.312 ± 0.044
93.3 ± 0.7	0.430 ± 0.052
Fe(p,6pXn)^{46}Sc (i)	
64.5 ± 1.3	0.051 ± 0.011
79.8 ± 0.9	1.33 ± 0.14
89.9 ± 0.9	1.85 ± 0.19
93.3 ± 0.7	1.75 ± 0.18
Fe(p,6pXn)^{47}Sc	
64.5 ± 1.3	0.154 ± 0.021
79.8 ± 0.9	0.267 ± 0.032
93.3 ± 0.7	0.260 ± 0.030
Fe(p,4pXn)^{48}V	
45.9 ± 1.7	3.58 ± 0.36
57.0 ± 1.2	6.10 ± 0.64
64.5 ± 1.3	5.01 ± 0.51
79.8 ± 0.9	8.42 ± 0.85
89.6 ± 0.7	16.2 ± 1.7
93.3 ± 0.7	16.8 ± 1.7
Fe(p,3pXn)^{51}Cr	
26.2 ± 3.1	0.869 ± 0.118
45.9 ± 1.7	89.6 ± 9.1
57.5 ± 1.6	60.7 ± 6.3
64.5 ± 1.3	45.5 ± 4.6
79.8 ± 0.9	61.6 ± 6.2
89.9 ± 0.9	77.2 ± 8.0
93.3 ± 0.7	70.9 ± 7.2
Fe(p,2pXn)^{52}Mn	
26.2 ± 3.1	19.8 ± 2.0
45.9 ± 1.7	14.0 ± 1.4
57.0 ± 1.2	14.1 ± 1.7
64.5 ± 1.3	31.3 ± 3.2
79.8 ± 0.9	36.0 ± 3.6
89.6 ± 0.7	28.8 ± 3.2
93.3 ± 0.7	29.7 ± 3.0
Fe(p,2pXn)^{54}Mn (i)	
26.2 ± 3.1	8.01 ± 0.81
45.9 ± 1.7	141. ± 14.
57.0 ± 1.2	102. ± 11.
64.5 ± 1.3	82.2 ± 8.3
79.8 ± 0.9	70.1 ± 7.1

Table 1 (continued): Cross sections [mb] for proton-induced reactions on Ti, V, Mn, Fe, Co, Ni, and Cu measured by γ-ray spectrometry. All cross sections are cumulative, except for those marked by "(i)" after the reaction as independent ones.

ENERGY [MeV]	CROSS SECTION [mb]
Fe(p,2pXn)^{54}Mn (i)	
89.6 ± 0.7	70.7 ± 7.3
93.3 ± 0.7	62.7 ± 6.3
Fe(p,Xn)^{56}Co (i)	
26.2 ± 3.1	29.8 ± 3.0
45.9 ± 1.7	12.1 ± 1.2
57.5 ± 1.6	9.74 ± 1.01
64.5 ± 1.3	8.09 ± 0.82
79.8 ± 0.9	6.28 ± 0.64
89.9 ± 0.9	5.53 ± 0.57
93.3 ± 0.7	5.00 ± 0.51
Fe(p,Xn)^{57}Co (i)	
26.2 ± 3.1	1.50 ± 0.15
45.9 ± 1.7	0.419 ± 0.046
57.5 ± 1.6	0.357 ± 0.038
64.5 ± 1.3	0.320 ± 0.036
79.8 ± 0.9	0.257 ± 0.030
89.9 ± 0.9	0.225 ± 0.024
93.3 ± 0.7	0.200 ± 0.024
Fe(p,Xn)^{58}Co (i)	
26.2 ± 3.1	0.111 ± 0.018
45.9 ± 1.7	0.049 ± 0.015
64.5 ± 1.3	0.037 ± 0.011
79.8 ± 0.9	0.034 ± 0.011
93.3 ± 0.7	0.031 ± 0.011
Co(p,7p7n)^{46}Sc (i)	
77.6 ± 1.0	0.161 ± 0.025
88.5 ± 1.0	0.307 ± 0.037
91.4 ± 0.7	0.296 ± 0.036
Co(p,5p7n)^{48}V	
77.6 ± 1.0	0.622 ± 0.065
91.4 ± 0.7	3.13 ± 0.32
Co(p,4p5n)^{51}Cr	
61.9 ± 1.3	2.81 ± 0.34
77.6 ± 1.0	16.3 ± 1.7
88.5 ± 1.0	31.1 ± 3.2
91.4 ± 0.7	29.2 ± 3.0
Co(p,3p5n)^{52}Mn	
61.9 ± 1.3	7.58 ± 0.77
77.6 ± 1.0	15.7 ± 1.6
91.4 ± 0.7	11.9 ± 1.2
Co(p,3p3n)^{54}Mn (i)	
42.6 ± 1.8	59.4 ± 6.0
55.7 ± 1.7	32.3 ± 3.4
61.9 ± 1.3	23.9 ± 2.4

ENERGY [MeV]	CROSS SECTION [mb]
Co(p,3p3n)^{54}Mn (i)	
77.6 ± 1.0	37.7 ± 3.8
88.5 ± 1.0	48.3 ± 5.0
91.4 ± 0.7	43.8 ± 4.4
Co(p,p3n)^{56}Co (i)	
42.6 ± 1.8	37.4 ± 3.8
55.7 ± 1.7	79.5 ± 8.2
61.9 ± 1.3	58.6 ± 5.9
77.6 ± 1.0	40.3 ± 4.1
88.5 ± 1.0	36.7 ± 3.8
91.4 ± 0.7	32.6 ± 3.3
Co(p,p2n)^{57}Co (i)	
42.6 ± 1.8	221. ± 25.
55.2 ± 1.2	169. ± 17.
61.9 ± 1.3	137. ± 14.
77.6 ± 1.0	111. ± 11.
88.2 ± 0.7	105. ± 11.
91.4 ± 0.7	92.8 ± 9.4
Co(p,pn)^{58}Co (i)	
42.6 ± 1.8	201. ± 20.
55.2 ± 1.2	182. ± 19.
61.9 ± 1.3	154. ± 16.
77.6 ± 1.0	135. ± 14.
88.2 ± 0.7	131. ± 14.
91.4 ± 0.7	114. ± 12.
Co(p,4n)^{56}Ni (i)	
42.6 ± 1.8	0.186 ± 0.020
61.9 ± 1.3	0.396 ± 0.041
77.6 ± 1.0	0.248 ± 0.026
91.4 ± 0.7	0.206 ± 0.022
Co(p,3n)^{57}Ni (i)	
42.6 ± 1.8	12.9 ± 1.3
61.9 ± 1.3	4.12 ± 0.43
77.6 ± 1.0	2.93 ± 0.31
91.4 ± 0.7	2.23 ± 0.23
Ni(p,6pXn)^{48}V	
76.2 ± 1.0	3.89 ± 0.40
90.1 ± 0.7	4.72 ± 0.48
Ni(p,5pXn)^{51}Cr	
40.4 ± 1.9	1.11 ± 0.25
52.5 ± 1.2	2.26 ± 0.37
60.2 ± 1.3	8.76 ± 0.92
76.2 ± 1.0	33.9 ± 3.5
86.3 ± 0.7	34.2 ± 3.6
90.1 ± 0.7	30.7 ± 3.1

ENERGY [MeV]	CROSS SECTION [mb]
Ni(p,4pXn)^{52}Mn	
40.4 ± 1.9	0.466 ± 0.052
60.2 ± 1.3	23.4 ± 2.4
76.2 ± 1.0	15.8 ± 1.6
90.1 ± 0.7	16.9 ± 1.7
Ni(p,4pXn)^{54}Mn (i)	
24.4 ± 3.2	0.108 ± 0.034
52.5 ± 1.2	8.04 ± 0.84
60.2 ± 1.3	15.8 ± 1.6
76.2 ± 1.0	23.4 ± 2.4
86.3 ± 0.7	23.6 ± 2.5
90.1 ± 0.7	21.2 ± 2.2
Ni(p,3pXn)^{59}Fe	
60.2 ± 1.3	0.139 ± 0.043
76.2 ± 1.0	0.119 ± 0.039
90.1 ± 0.7	0.166 ± 0.038
Ni(p,2pXn)^{56}Co (i)	
24.4 ± 3.2	15.3 ± 1.5
40.4 ± 1.9	206. ± 21.
52.5 ± 1.2	133. ± 14.
60.2 ± 1.3	107. ± 11.
76.2 ± 1.0	96.4 ± 9.8
86.3 ± 0.7	92.7 ± 9.6
90.1 ± 0.7	84.1 ± 8.5
Ni(p,2pXn)^{57}Co (i)	
24.4 ± 3.2	477. ± 48.
40.4 ± 1.9	190. ± 19.
52.5 ± 1.2	206. ± 21.
60.2 ± 1.3	175. ± 18.
76.2 ± 1.0	148. ± 15.
86.3 ± 0.7	142. ± 15.
90.1 ± 0.7	128. ± 13.
Ni(p,2pXn)^{58}Co (i)	
24.4 ± 3.2	7.96 ± 0.81
40.4 ± 1.9	66.0 ± 6.7
52.5 ± 1.2	49.9 ± 5.2
60.2 ± 1.3	38.7 ± 3.9
76.2 ± 1.0	34.5 ± 3.5
86.3 ± 0.7	35.8 ± 3.7
90.1 ± 0.7	30.6 ± 3.1
Ni(p,2pXn)^{60}Co	
24.4 ± 3.2	0.908 ± 0.184
52.5 ± 1.2	2.15 ± 0.27
60.2 ± 1.3	2.09 ± 0.33
76.2 ± 1.0	1.90 ± 0.30

Table 1 (continued): Cross sections [mb] for proton-induced reactions on Ti, V, Mn, Fe, Co, Ni, and Cu measured by γ-ray spectrometry. All cross sections are cumulative, except for those marked by "(i)" after the reaction as independent ones.

ENERGY [MeV]	CROSS SECTION [mb]
Ni(p,2pXn)^{60}Co	
86.3 ± 0.7	2.00 ± 0.24
90.1 ± 0.7	2.00 ± 0.28
Ni(p,pXn)^{56}Ni	
24.4 ± 3.2	0.921 ± 0.094
40.4 ± 1.9	11.3 ± 1.2
60.2 ± 1.3	8.19 ± 0.83
76.2 ± 1.0	7.49 ± 0.76
90.1 ± 0.7	6.74 ± 0.68
Ni(p,pXn)^{57}Ni	
24.4 ± 3.2	161. ± 16.
40.4 ± 1.9	84.9 ± 8.6
60.2 ± 1.3	72.9 ± 7.4
76.2 ± 1.0	65.9 ± 6.7
90.1 ± 0.7	60.1 ± 6.1
Cu(p,6pXn)^{51}Cr	
57.6 ± 1.4	0.281 ± 0.055
74.0 ± 1.0	0.332 ± 0.064
85.3 ± 1.1	0.694 ± 0.086
88.1 ± 0.8	0.926 ± 0.115
Cu(p,5pXn)^{52}Mn	
74.0 ± 1.0	0.225 ± 0.028
84.9 ± 0.8	1.39 ± 0.14
88.1 ± 0.8	1.62 ± 0.17
Cu(p,5pXn)^{54}Mn (i)	
51.0 ± 1.8	2.28 ± 0.24
57.6 ± 1.4	4.19 ± 0.43
74.0 ± 1.0	3.39 ± 0.34
85.3 ± 1.1	5.35 ± 0.56
88.1 ± 0.8	5.80 ± 0.59
Cu(p,4pXn)^{59}Fe	
51.0 ± 1.8	0.279 ± 0.030
57.6 ± 1.4	0.543 ± 0.057
74.0 ± 1.0	0.767 ± 0.080
85.3 ± 1.1	0.872 ± 0.093
88.1 ± 0.8	0.834 ± 0.086
Cu(p,3pXn)^{55}Co	
74.0 ± 1.0	0.816 ± 0.160
84.9 ± 0.8	1.64 ± 0.17
88.1 ± 0.8	1.95 ± 0.30
Cu(p,3pXn)^{56}Co (i)	
51.0 ± 1.8	0.445 ± 0.074
57.6 ± 1.4	3.48 ± 0.35
74.0 ± 1.0	13.4 ± 1.4
85.3 ± 1.1	11.7 ± 1.2
88.1 ± 0.8	13.5 ± 1.0

ENERGY [MeV]	CROSS SECTION [mb]
Cu(p,3pXn)^{57}Co (i)	
22.5 ± 3.4	0.033 ± 0.014
36.8 ± 2.1	1.10 ± 0.11
51.0 ± 1.8	53.0 ± 5.5
57.6 ± 1.4	48.9 ± 4.9
74.0 ± 1.0	32.7 ± 3.3
85.3 ± 1.1	39.8 ± 4.1
88.1 ± 0.8	38.7 ± 3.9
Cu(p,3pXn)^{58}Co (i)	
22.5 ± 3.4	0.192 ± 0.021
36.8 ± 2.1	52.7 ± 5.3
51.0 ± 1.8	37.6 ± 3.9
57.6 ± 1.4	30.0 ± 3.0
74.0 ± 1.0	45.7 ± 4.6
85.3 ± 1.1	56.3 ± 5.8
88.1 ± 0.8	51.5 ± 5.2
Cu(p,3pXn)^{60}Co	
36.8 ± 2.1	5.42 ± 0.56
51.0 ± 1.8	11.1 ± 1.1
57.6 ± 1.4	11.0 ± 1.1
74.0 ± 1.0	10.4 ± 1.1
85.3 ± 1.1	11.7 ± 1.2
88.1 ± 0.8	11.2 ± 1.1
Cu(p,2pXn)^{56}Ni	
74.0 ± 1.0	0.086 ± 0.011
84.9 ± 0.8	0.075 ± 0.008
88.1 ± 0.8	0.066 ± 0.010
Cu(p,2pXn)^{57}Ni	
36.8 ± 2.1	0.046 ± 0.012
50.5 ± 1.3	1.87 ± 0.19
57.6 ± 1.4	2.38 ± 0.25
74.0 ± 1.0	1.21 ± 0.13
84.9 ± 0.8	1.41 ± 0.15
88.1 ± 0.8	1.54 ± 0.16
Cu(p,pXn)^{64}Cu (i)	
22.5 ± 3.4	106. ± 15.
36.8 ± 2.1	70.0 ± 11.9
50.5 ± 1.3	58.1 ± 6.1
57.6 ± 1.4	59.3 ± 12.8
74.0 ± 1.0	52.0 ± 11.3
84.9 ± 0.8	41.5 ± 4.4
88.1 ± 0.8	41.3 ± 9.6

ENERGY [MeV]	CROSS SECTION [mb]
Cu(p,Xn)^{62}Zn (i)	
22.5 ± 3.4	67.5 ± 6.9
36.8 ± 2.1	15.8 ± 1.8
50.5 ± 1.3	13.1 ± 1.4
57.6 ± 1.4	9.73 ± 1.27
74.0 ± 1.0	6.92 ± 1.02
84.9 ± 0.8	5.52 ± 0.57
88.1 ± 0.8	5.13 ± 0.95
Cu(p,Xn)^{65}Zn (i)	
22.5 ± 3.4	18.1 ± 1.9
36.8 ± 2.1	7.08 ± 0.72
51.0 ± 1.3	5.23 ± 0.54
57.6 ± 1.4	3.82 ± 0.39
74.0 ± 1.0	2.86 ± 0.29
85.3 ± 1.1	2.78 ± 0.29
88.1 ± 0.8	2.46 ± 0.26

Table 2: Cross sections [mb] for the reaction $^{27}Al(p,3pn)^{22}Na$.

ENERGY [MeV]	CROSS SECTION [mb]	
24.7 ± 0.6	0.010 ± 0.005	PSI
26.6 ± 0.8	0.208 ± 0.011	PSI
29.1 ± 0.8	1.69 ± 0.09	PSI
29.6 ± 0.6	1.64 ± 0.09	PSI
31.4 ± 0.8	7.06 ± 0.36	PSI
31.6 ± 2.5	7.24 ± 0.74	TSL
32.8 ± 0.7	11.5 ± 0.6	PSI
33.2 ± 0.7	14.8 ± 0.8	PSI
33.6 ± 0.7	16.3 ± 0.8	PSI
33.6 ± 0.9	11.0 ± 0.6	PSI
33.8 ± 0.7	16.6 ± 0.9	PSI
33.9 ± 0.5	13.8 ± 0.7	PSI
34.5 ± 0.7	18.9 ± 1.0	PSI
35.4 ± 0.7	23.2 ± 1.2	PSI
35.7 ± 0.7	26.2 ± 1.3	PSI
37.7 ± 0.7	33.9 ± 1.7	PSI
37.8 ± 0.9	31.1 ± 1.6	PSI
37.9 ± 0.4	31.3 ± 1.7	PSI
38.6 ± 0.9	34.5 ± 1.8	PSI
39.0 ± 0.9	36.9 ± 1.9	PSI
39.7 ± 0.6	39.0 ± 2.0	PSI
40.7 ± 0.9	38.6 ± 2.0	PSI
41.1 ± 0.6	40.8 ± 2.1	PSI
41.5 ± 0.4	42.5 ± 2.3	PSI
41.5 ± 0.6	41.8 ± 2.1	PSI
43.3 ± 0.6	43.6 ± 2.2	PSI
43.4 ± 0.6	42.9 ± 2.3	PSI
43.4 ± 0.6	42.4 ± 2.2	PSI
43.6 ± 0.9	44.0 ± 2.2	PSI
43.7 ± 0.6	43.5 ± 2.2	PSI
44.1 ± 0.6	43.0 ± 2.2	PSI
44.6 ± 0.9	42.7 ± 2.2	PSI
44.9 ± 0.3	44.5 ± 2.5	PSI
46.3 ± 0.8	41.4 ± 2.1	PSI
47.9 ± 0.8	39.4 ± 2.0	PSI
48.0 ± 0.8	40.4 ± 2.0	PSI
49.6 ± 0.8	38.1 ± 1.9	PSI
51.2 ± 0.8	36.4 ± 1.8	PSI
51.8 ± 0.8	34.8 ± 1.8	PSI
52.7 ± 0.8	34.9 ± 1.8	PSI
53.2 ± 0.8	31.5 ± 1.6	PSI
54.0 ± 1.4	33.3 ± 3.4	TSL
54.2 ± 0.8	32.3 ± 1.6	PSI
54.7 ± 0.8	29.8 ± 1.6	PSI
55.3 ± 0.7	30.8 ± 1.6	PSI
55.3 ± 0.8	29.5 ± 1.5	PSI
55.7 ± 0.8	30.2 ± 1.5	PSI
55.7 ± 0.8	30.1 ± 1.5	PSI
57.2 ± 0.7	29.1 ± 1.5	PSI
58.1 ± 0.7	26.6 ± 1.4	PSI
58.3 ± 0.7	27.4 ± 1.4	PSI
58.7 ± 0.7	27.0 ± 1.4	PSI
60.2 ± 0.7	26.7 ± 1.4	PSI
61.6 ± 0.7	25.7 ± 1.3	PSI
61.9 ± 0.6	25.2 ± 1.3	PSI
62.9 ± 1.2	26.0 ± 3.0	TSL
62.9 ± 0.7	24.8 ± 1.3	PSI
64.3 ± 0.7	24.4 ± 1.2	PSI
64.9 ± 0.5	23.8 ± 1.2	PSI
65.6 ± 0.6	23.3 ± 1.2	PSI
66.9 ± 0.6	22.6 ± 1.1	PSI
67.9 ± 0.5	23.0 ± 1.2	PSI
68.2 ± 0.6	22.5 ± 1.1	PSI
68.2 ± 0.6	21.5 ± 1.1	PSI
68.3 ± 0.6	21.6 ± 1.1	PSI
69.4 ± 0.6	22.0 ± 1.1	PSI
70.8 ± 0.4	22.2 ± 1.1	PSI
70.8 ± 0.6	20.9 ± 1.1	PSI
70.8 ± 0.6	21.9 ± 1.1	PSI
70.8 ± 0.6	22.0 ± 1.1	PSI
70.9 ± 0.6	21.8 ± 1.1	PSI
71.0 ± 0.9	22.8 ± 2.3	TSL
85.6 ± 0.7	20.9 ± 2.1	TSL
93.9 ± 0.5	20.8 ± 2.3	TSL
98.5 ± 0.3	19.8 ± 2.0	TSL
256. ± 1.3	14.3 ± 0.8	LNS
297. ± 0.6	15.4 ± 0.8	LNS
298. ± 0.6	13.4 ± 1.7	LNS
362. ± 1.3	15.7 ± 1.3	LNS
398. ± 0.6	16.1 ± 1.0	LNS
600.	16.0 ± 1.0	LNS
800.	15.1 ± 1.1	LNS
1200.	14.5 ± 1.0	LNS
1600.	13.1 ± 1.0	LNS
2600.	12.1 ± 0.9	LNS

Table 3: Cross sections [mb] for the reaction $^{27}Al(p,X)^{7}Be$.

ENERGY [MeV]	CROSS SECTION [mb]		ENERGY [MeV]	CROSS SECTION [mb]		ENERGY [MeV]	CROSS SECTION [mb]	
23.9 ± 0.8	0.0044 ± 0.0018	PSI	64.3 ± 0.7	0.617 ± 0.048	PSI	275. ± 1.0	2.13 ± 0.16	LNS
26.6 ± 0.8	0.0140 ± 0.0038	PSI	64.9 ± 0.5	0.614 ± 0.033	PSI	278. ± 0.9	2.12 ± 0.17	LNS
29.1 ± 0.8	0.0387 ± 0.0056	PSI	65.6 ± 0.6	0.635 ± 0.034	PSI	281. ± 0.9	2.15 ± 0.17	LNS
31.4 ± 0.8	0.0735 ± 0.0105	PSI	66.9 ± 0.6	0.649 ± 0.034	PSI	283. ± 0.9	2.18 ± 0.17	LNS
31.6 ± 2.5	0.0613 ± 0.0184	TSL	67.9 ± 0.5	0.668 ± 0.054	PSI	285. ± 0.8	2.22 ± 0.17	LNS
33.2 ± 0.7	0.0792 ± 0.0328	PSI	68.2 ± 0.6	0.668 ± 0.034	PSI	286. ± 0.8	2.31 ± 0.18	LNS
33.6 ± 0.9	0.0808 ± 0.0077	PSI	68.2 ± 0.6	0.654 ± 0.037	PSI	289. ± 0.7	2.35 ± 0.17	LNS
33.9 ± 0.5	0.0810 ± 0.017	PSI	68.3 ± 0.6	0.652 ± 0.039	PSI	292. ± 0.7	2.37 ± 0.18	LNS
35.7 ± 0.7	0.163 ± 0.035	PSI	69.4 ± 0.6	0.694 ± 0.036	PSI	295. ± 0.6	2.39 ± 0.18	LNS
36.4 ± 0.9	0.130 ± 0.010	PSI	70.8 ± 0.4	0.717 ± 0.037	PSI	296. ± 0.6	2.43 ± 0.19	LNS
37.8 ± 0.9	0.163 ± 0.017	PSI	70.8 ± 0.6	0.676 ± 0.036	PSI	297. ± 0.6	2.29 ± 0.13	LNS
37.9 ± 0.4	0.145 ± 0.023	PSI	70.8 ± 0.6	0.718 ± 0.038	PSI	298. ± 0.6	2.32 ± 0.18	LNS
38.4 ± 0.9	0.161 ± 0.014	PSI	70.8 ± 0.6	0.713 ± 0.037	PSI	298. ± 0.6	2.46 ± 0.19	LNS
38.6 ± 0.9	0.164 ± 0.014	PSI	70.9 ± 0.6	0.702 ± 0.038	PSI	298. ± 0.6	2.57 ± 0.43	LNS
39.0 ± 0.9	0.220 ± 0.043	PSI	71.0 ± 0.9	0.692 ± 0.078	TSL	325. ± 1.6	2.62 ± 0.20	LNS
39.4 ± 0.9	0.148 ± 0.011	PSI	85.6 ± 0.7	0.829 ± 0.090	TSL	326. ± 1.6	2.44 ± 0.32	LNS
39.7 ± 0.6	0.209 ± 0.025	PSI	93.9 ± 0.5	0.980 ± 0.115	TSL	328. ± 1.6	2.64 ± 0.21	LNS
40.7 ± 0.9	0.187 ± 0.026	PSI	98.5 ± 0.3	0.912 ± 0.098	TSL	329. ± 1.6	2.62 ± 0.23	LNS
41.5 ± 0.4	0.186 ± 0.026	PSI	211. ± 1.6	1.70 ± 0.24	LNS	330. ± 1.6	2.70 ± 0.21	LNS
41.5 ± 0.6	0.211 ± 0.029	PSI	212. ± 1.6	1.89 ± 0.23	LNS	333. ± 1.6	2.74 ± 0.31	LNS
43.3 ± 0.6	0.272 ± 0.050	PSI	214. ± 1.6	1.51 ± 0.18	LNS	334. ± 1.5	2.69 ± 0.21	LNS
43.6 ± 0.9	0.303 ± 0.016	PSI	215. ± 1.6	1.87 ± 0.23	LNS	335. ± 1.5	2.65 ± 0.21	LNS
43.7 ± 0.6	0.230 ± 0.061	PSI	217. ± 1.6	1.69 ± 0.25	LNS	335. ± 1.5	2.70 ± 0.27	LNS
44.6 ± 0.9	0.318 ± 0.056	PSI	221. ± 1.6	1.72 ± 0.22	LNS	336. ± 1.5	2.62 ± 0.34	LNS
44.9 ± 0.3	0.265 ± 0.035	PSI	222. ± 1.5	1.78 ± 0.20	LNS	339. ± 1.5	2.70 ± 0.20	LNS
46.3 ± 0.8	0.306 ± 0.025	PSI	223. ± 1.5	1.85 ± 0.23	LNS	342. ± 1.5	2.31 ± 0.37	LNS
47.9 ± 0.8	0.344 ± 0.050	PSI	223. ± 1.5	1.55 ± 0.19	LNS	344. ± 1.4	2.74 ± 0.21	LNS
48.0 ± 0.8	0.337 ± 0.029	PSI	225. ± 1.5	1.66 ± 0.22	LNS	347. ± 1.4	2.67 ± 0.26	LNS
49.6 ± 0.8	0.363 ± 0.041	PSI	228. ± 1.5	1.83 ± 0.17	LNS	349. ± 1.4	2.79 ± 0.21	LNS
51.2 ± 0.8	0.414 ± 0.041	PSI	231. ± 1.5	2.00 ± 0.27	LNS	351. ± 1.4	2.76 ± 0.24	LNS
51.8 ± 0.8	0.421 ± 0.022	PSI	240. ± 1.4	1.98 ± 0.23	LNS	351. ± 1.4	2.88 ± 0.22	LNS
52.7 ± 0.9	0.409 ± 0.045	PSI	242. ± 1.4	1.80 ± 0.31	LNS	355. ± 1.3	3.03 ± 0.25	LNS
53.2 ± 0.8	0.431 ± 0.028	PSI	243. ± 1.3	1.70 ± 0.15	LNS	357. ± 1.3	2.66 ± 0.21	LNS
54.0 ± 1.4	0.521 ± 0.066	TSL	247. ± 1.3	1.85 ± 0.22	LNS	360. ± 1.3	2.76 ± 0.26	LNS
54.2 ± 0.8	0.424 ± 0.046	PSI	253. ± 1.3	2.02 ± 0.23	LNS	361. ± 1.2	2.92 ± 0.23	LNS
54.7 ± 0.8	0.453 ± 0.027	PSI	255. ± 1.2	1.87 ± 0.20	LNS	362. ± 1.2	3.02 ± 0.28	LNS
55.3 ± 0.7	0.471 ± 0.050	PSI	256. ± 1.2	1.99 ± 0.21	LNS	362. ± 1.3	2.86 ± 0.02	LNS
55.3 ± 0.8	0.440 ± 0.025	PSI	256. ± 1.3	1.82 ± 0.12	LNS	363. ± 1.2	2.96 ± 0.22	LNS
55.7 ± 0.8	0.462 ± 0.030	PSI	257. ± 1.2	1.85 ± 0.20	LNS	363. ± 1.2	2.86 ± 0.22	LNS
55.7 ± 0.8	0.475 ± 0.026	PSI	258. ± 1.2	1.92 ± 0.15	LNS	364. ± 1.2	2.80 ± 0.22	LNS
57.2 ± 0.7	0.487 ± 0.047	PSI	260. ± 1.2	2.04 ± 0.16	LNS	365. ± 1.2	2.95 ± 0.23	LNS
58.1 ± 0.7	0.481 ± 0.028	PSI	261. ± 1.2	1.87 ± 0.14	LNS	366. ± 1.2	2.89 ± 0.23	LNS
58.3 ± 0.7	0.512 ± 0.027	PSI	263. ± 1.1	2.05 ± 0.16	LNS	368. ± 1.2	3.03 ± 0.23	LNS
58.7 ± 0.6	0.539 ± 0.027	PSI	266. ± 1.1	2.07 ± 0.16	LNS	370. ± 1.1	3.01 ± 0.23	LNS
60.2 ± 0.7	0.536 ± 0.046	PSI	267. ± 1.1	2.06 ± 0.16	LNS	371. ± 1.1	3.01 ± 0.23	LNS
61.6 ± 0.7	0.532 ± 0.049	PSI	268. ± 1.1	2.14 ± 0.18	LNS	372. ± 1.1	3.01 ± 0.24	LNS
61.9 ± 0.6	0.605 ± 0.050	PSI	268. ± 1.1	2.00 ± 0.17	LNS	372. ± 1.1	2.95 ± 0.23	LNS
62.9 ± 1.2	0.629 ± 0.081	TSL	270. ± 1.1	2.06 ± 0.17	LNS	374. ± 1.1	3.01 ± 0.22	LNS
62.9 ± 0.7	0.566 ± 0.043	PSI	273. ± 1.0	2.14 ± 0.18	LNS	376. ± 1.0	3.15 ± 0.23	LNS

Table 3 (continued): Cross sections [mb] for the reaction $^{27}Al(p,X)^{7}Be$.

ENERGY [MeV]	CROSS SECTION [mb]		ENERGY [MeV]	CROSS SECTION [mb]		ENERGY [MeV]	CROSS SECTION [mb]	
379. ± 1.0	3.07 ± 0.23	LNS	391. ± 0.7	3.23 ± 0.24	LNS	398. ± 0.6	3.34 ± 0.27	LNS
381. ± 0.9	3.10 ± 0.25	LNS	393. ± 0.7	3.21 ± 0.23	LNS	600.	4.88 ± 0.31	LNS
383. ± 0.9	3.00 ± 0.23	LNS	396. ± 0.6	3.30 ± 0.25	LNS	800.	6.43 ± 0.46	LNS
385. ± 0.9	3.08 ± 0.23	LNS	397. ± 0.6	3.36 ± 0.26	LNS	1200.	8.48 ± 0.63	LNS
387. ± 0.9	3.22 ± 0.25	LNS	398. ± 0.6	3.26 ± 0.25	LNS	1600.	8.65 ± 0.63	LNS
388. ± 0.8	3.21 ± 0.23	LNS	398. ± 0.6	3.32 ± 0.25	LNS	2600.	9.50 ± 0.72	LNS

Table 4: Cross sections [mb] for the reaction $^{27}Al(p,3pn)^{24}Na$.

ENERGY [MeV]	CROSS SECTION [mb]		ENERGY [MeV]	CROSS SECTION [mb]		ENERGY [MeV]	CROSS SECTION [mb]	
24.7 ± 0.6	0.048 ± 0.018	PSI	48.0 ± 0.8	5.16 ± 0.26	PSI	211. ± 1.6	8.59 ± 0.71	LNS
29.6 ± 0.6	0.085 ± 0.019	PSI	49.6 ± 0.8	6.23 ± 0.32	PSI	212. ± 1.6	9.11 ± 0.75	LNS
31.4 ± 0.8	0.376 ± 0.020	PSI	51.2 ± 0.8	7.14 ± 0.36	PSI	214. ± 1.6	9.33 ± 0.81	LNS
32.8 ± 0.7	0.373 ± 0.020	PSI	51.8 ± 0.8	7.98 ± 0.41	PSI	215. ± 1.6	9.25 ± 0.75	LNS
33.2 ± 0.7	0.472 ± 0.024	PSI	52.7 ± 0.8	7.93 ± 0.40	PSI	217. ± 1.6	9.30 ± 0.77	LNS
33.6 ± 0.7	0.637 ± 0.033	PSI	53.2 ± 0.8	8.09 ± 0.43	PSI	221. ± 1.6	9.56 ± 0.77	LNS
33.6 ± 0.9	0.606 ± 0.034	PSI	54.2 ± 0.8	8.89 ± 0.45	PSI	222. ± 1.5	8.88 ± 0.76	LNS
33.8 ± 0.7	0.534 ± 0.028	PSI	54.7 ± 0.8	9.21 ± 0.50	PSI	223. ± 1.5	9.31 ± 0.79	LNS
33.9 ± 0.5	0.342 ± 0.029	PSI	55.3 ± 0.7	10.1 ± 0.5	PSI	223. ± 1.5	8.92 ± 0.78	LNS
34.5 ± 0.7	0.525 ± 0.028	PSI	55.3 ± 0.8	9.05 ± 0.46	PSI	225. ± 1.5	8.51 ± 0.71	LNS
35.4 ± 0.7	0.666 ± 0.036	PSI	55.7 ± 0.8	9.70 ± 0.49	PSI	228. ± 1.5	8.73 ± 0.73	LNS
35.7 ± 0.7	0.837 ± 0.048	PSI	55.7 ± 0.8	9.70 ± 0.50	PSI	231. ± 1.5	9.37 ± 0.82	LNS
36.4 ± 0.9	0.866 ± 0.045	PSI	57.2 ± 0.7	10.3 ± 0.5	PSI	234. ± 1.4	10.0 ± 0.8	LNS
37.7 ± 0.7	1.34 ± 0.07	PSI	58.1 ± 0.7	10.3 ± 0.5	PSI	237. ± 1.4	9.22 ± 0.72	LNS
37.8 ± 0.9	1.29 ± 0.07	PSI	58.3 ± 0.7	10.6 ± 0.6	PSI	240. ± 1.4	9.42 ± 0.74	LNS
37.9 ± 0.4	0.94 ± 0.06	PSI	58.7 ± 0.6	10.7 ± 0.5	PSI	242. ± 1.4	9.03 ± 0.76	LNS
38.4 ± 0.9	1.24 ± 0.06	PSI	60.2 ± 0.7	11.0 ± 0.6	PSI	243. ± 1.4	9.65 ± 0.74	LNS
38.6 ± 0.9	1.41 ± 0.07	PSI	61.6 ± 0.7	11.5 ± 0.6	PSI	247. ± 1.3	9.76 ± 0.72	LNS
39.0 ± 0.9	1.64 ± 0.08	PSI	61.9 ± 0.6	11.6 ± 0.6	PSI	253. ± 1.3	10.1 ± 0.7	LNS
39.4 ± 0.9	1.19 ± 0.06	PSI	62.9 ± 0.7	11.7 ± 0.6	PSI	255. ± 1.2	10.1 ± 0.8	LNS
39.7 ± 0.6	1.77 ± 0.09	PSI	63.0 ± 0.9	13.3 ± 1.4	TSL	256. ± 1.2	9.88 ± 0.71	LNS
40.7 ± 0.9	1.75 ± 0.09	PSI	64.3 ± 0.7	11.7 ± 0.6	PSI	257. ± 1.2	9.71 ± 0.80	LNS
41.1 ± 0.6	1.76 ± 0.09	PSI	64.9 ± 0.5	11.4 ± 0.6	PSI	260. ± 1.2	9.77 ± 0.80	LNS
41.5 ± 0.4	1.80 ± 0.11	PSI	65.6 ± 0.6	11.7 ± 0.6	PSI	263. ± 1.1	9.88 ± 0.79	LNS
41.5 ± 0.6	2.26 ± 0.12	PSI	66.9 ± 0.6	11.9 ± 0.6	PSI	267. ± 1.1	10.5 ± 0.9	LNS
43.3 ± 0.6	2.66 ± 0.14	PSI	68.2 ± 0.6	11.8 ± 0.6	PSI	268. ± 1.1	9.79 ± 0.84	LNS
43.4 ± 0.6	2.66 ± 0.14	PSI	68.2 ± 0.6	11.3 ± 0.6	PSI	273. ± 1.0	9.48 ± 0.79	LNS
43.4 ± 0.6	2.63 ± 0.13	PSI	68.3 ± 0.6	10.9 ± 0.7	PSI	278. ± 0.9	9.85 ± 0.80	LNS
43.6 ± 0.9	3.60 ± 0.18	PSI	69.4 ± 0.6	11.6 ± 0.6	PSI	283. ± 0.9	11.0 ± 0.8	LNS
43.7 ± 0.6	2.86 ± 0.14	PSI	70.8 ± 0.4	11.7 ± 0.6	PSI	286. ± 0.8	11.1 ± 0.8	LNS
44.1 ± 0.6	2.94 ± 0.15	PSI	70.8 ± 0.4	11.4 ± 0.6	PSI	292. ± 0.7	10.7 ± 0.8	LNS
44.6 ± 0.9	3.12 ± 0.16	PSI	70.8 ± 0.6	11.4 ± 0.6	PSI	296. ± 0.6	10.4 ± 0.8	LNS
44.9 ± 0.3	3.14 ± 0.18	PSI	70.8 ± 0.6	11.6 ± 0.6	PSI	297. ± 0.6	10.5 ± 0.6	LNS
46.3 ± 0.8	3.98 ± 0.20	PSI	70.9 ± 0.6	11.4 ± 0.6	PSI	298. ± 0.6	11.0 ± 0.8	LNS
47.9 ± 0.8	5.73 ± 0.29	PSI	94.0 ± 0.4	12.0 ± 1.2	TSL	298. ± 0.6	11.2 ± 0.6	LNS

Table 4: (continued): Cross sections [mb] for the reaction $^{27}Al(p,3pn)^{24}Na$.

ENERGY [MeV]	CROSS SECTION [mb]		ENERGY [MeV]	CROSS SECTION [mb]		ENERGY [MeV]	CROSS SECTION [mb]	
325. ± 1.6	9.77 ± 0.80	LNS	357. ± 1.3	10.7 ± 0.8	LNS	381. ± 0.9	10.3 ± 0.9	LNS
326. ± 1.6	10.1 ± 0.9	LNS	360. ± 1.3	11.0 ± 0.8	LNS	383. ± 0.9	10.2 ± 0.8	LNS
328. ± 1.6	9.97 ± 0.82	LNS	361. ± 1.2	10.8 ± 0.8	LNS	385. ± 0.9	10.6 ± 0.8	LNS
329. ± 1.6	10.1 ± 0.8	LNS	362. ± 1.3	11.3 ± 0.9	LNS	387. ± 0.8	11.6 ± 0.9	LNS
330. ± 1.6	9.98 ± 1.17	LNS	362. ± 1.2	11.4 ± 0.8	LNS	388. ± 0.8	11.0 ± 0.8	LNS
333. ± 1.6	10.4 ± 0.8	LNS	363. ± 1.2	10.2 ± 0.8	LNS	391. ± 0.7	11.9 ± 0.9	LNS
334. ± 1.5	9.87 ± 0.81	LNS	363. ± 1.2	10.9 ± 0.8	LNS	393. ± 0.7	11.2 ± 0.8	LNS
335. ± 1.5	9.73 ± 0.82	LNS	364. ± 1.2	10.4 ± 0.9	LNS	396. ± 0.6	11.8 ± 0.9	LNS
335. ± 1.5	10.5 ± 0.9	LNS	365. ± 1.2	10.5 ± 0.9	LNS	397. ± 0.6	10.7 ± 0.8	LNS
336. ± 1.5	10.0 ± 0.8	LNS	366. ± 1.2	11.0 ± 0.9	LNS	398. ± 0.6	11.7 ± 0.9	LNS
339. ± 1.5	9.50 ± 0.79	LNS	368. ± 1.2	10.6 ± 0.9	LNS	398. ± 0.6	11.3 ± 0.9	LNS
342. ± 1.5	9.81 ± 0.83	LNS	370. ± 1.1	10.2 ± 0.8	LNS	398. ± 0.6	11.7 ± 1.1	LNS
344. ± 1.4	9.98 ± 0.81	LNS	371. ± 1.1	10.6 ± 0.9	LNS	600.	11.3 ± 0.7	LNS
347. ± 1.4	10.1 ± 0.8	LNS	372. ± 1.1	11.5 ± 1.0	LNS	800.	11.2 ± 0.8	LNS
349. ± 1.4	10.2 ± 0.8	LNS	372. ± 1.1	10.5 ± 0.9	LNS	1200.	10.8 ± 0.8	LNS
351. ± 1.4	11.1 ± 0.9	LNS	374. ± 1.1	10.3 ± 0.9	LNS	1600.	12.3 ± 1.0	LNS
351. ± 1.4	10.6 ± 0.8	LNS	376. ± 1.0	9.64 ± 0.81	LNS	2600.	10.6 ± 0.8	LNS
355. ± 1.3	11.4 ± 0.9	LNS	379. ± 1.0	10.9 ± 0.9	LNS			

Table 5: Cross sections [mb] for the reaction $Cu_{nat}(p,n)^{65}Zn$. Note that the cross sections are given for natural copper though ^{65}Zn can only be produced by the reaction $^{65}Cu(p,n)^{65}Zn$.

ENERGY [MeV]	CROSS SECTION [mb]		ENERGY [MeV]	CROSS SECTION [mb]		ENERGY [MeV]	CROSS SECTION [mb]	
8.8 ± 1.2	201. ± 10.	PSI	20.7 ± 0.9	16.6 ± 0.9	PSI	30.1 ± 0.8	8.41 ± 0.44	PSI
10.1 ± 1.1	202. ± 11.	PSI	21.1 ± 0.9	16.1 ± 0.8	PSI	30.1 ± 0.8	8.51 ± 0.43	PSI
12.0 ± 1.1	133. ± 7.	PSI	21.2 ± 0.9	15.9 ± 0.8	PSI	30.2 ± 0.8	8.53 ± 0.44	PSI
12.9 ± 1.1	137. ± 7.	PSI	22.4 ± 0.9	13.7 ± 0.7	PSI	30.4 ± 0.8	8.30 ± 0.47	PSI
14.4 ± 1.0	102. ± 5.	PSI	22.4 ± 0.9	14.1 ± 0.8	PSI	32.2 ± 0.7	7.88 ± 0.44	PSI
15.0 ± 1.0	59.5 ± 3.1	PSI	22.5 ± 3.4	18.1 ± 1.9	TSL	32.2 ± 0.8	7.85 ± 0.42	PSI
15.0 ± 1.0	59.5 ± 3.0	PSI	23.2 ± 0.9	12.3 ± 0.6	PSI	32.5 ± 0.7	7.84 ± 0.40	PSI
15.4 ± 1.0	64.1 ± 3.7	PSI	23.7 ± 0.9	12.2 ± 0.7	PSI	32.7 ± 0.7	7.65 ± 0.40	PSI
15.8 ± 1.0	46.5 ± 2.4	PSI	24.2 ± 0.8	11.7 ± 0.6	PSI	32.8 ± 0.7	7.75 ± 0.41	PSI
16.7 ± 1.0	37.2 ± 1.9	PSI	24.6 ± 0.8	11.6 ± 0.6	PSI	33.4 ± 0.7	7.57 ± 0.40	PSI
16.8 ± 1.0	40.1 ± 2.1	PSI	25.3 ± 0.8	10.7 ± 0.6	PSI	33.9 ± 0.7	7.43 ± 0.41	PSI
17.4 ± 0.9	31.2 ± 1.6	PSI	25.6 ± 0.8	10.3 ± 0.5	PSI	34.6 ± 0.9	7.56 ± 0.40	PSI
17.4 ± 0.9	39.3 ± 2.2	PSI	25.9 ± 0.8	10.2 ± 0.6	PSI	34.7 ± 0.7	7.13 ± 0.37	PSI
17.5 ± 1.0	28.9 ± 1.5	PSI	26.7 ± 0.8	10.3 ± 0.6	PSI	34.8 ± 0.7	7.05 ± 0.36	PSI
18.2 ± 0.9	26.1 ± 1.3	PSI	26.8 ± 0.8	9.55 ± 0.50	PSI	35.2 ± 0.7	7.09 ± 0.37	PSI
18.5 ± 0.9	26.2 ± 1.5	PSI	27.3 ± 0.8	9.61 ± 0.53	PSI	36.2 ± 0.7	6.80 ± 0.38	PSI
19.5 ± 0.9	20.1 ± 1.0	PSI	27.8 ± 0.8	9.55 ± 0.49	PSI	36.7 ± 0.7	6.73 ± 0.35	PSI
19.7 ± 0.9	20.3 ± 1.0	PSI	27.9 ± 0.8	9.33 ± 0.48	PSI	36.7 ± 0.7	6.76 ± 0.35	PSI
20.0 ± 0.9	20.7 ± 1.1	PSI	28.1 ± 0.8	9.44 ± 0.50	PSI	36.8 ± 2.1	7.08 ± 0.72	TSL
20.5 ± 0.9	16.5 ± 0.9	PSI	28.6 ± 0.8	9.24 ± 0.51	PSI	36.9 ± 0.7	6.55 ± 0.40	PSI

Table 5 (continued): Cross sections [mb] for the reaction $Cu_{nat}(p,n)^{65}Zn$. Note that the cross sections are given for natural copper though ^{65}Zn can only be produced by the reaction $^{65}Cu(p,n)^{65}Zn$.

ENERGY [MeV]	CROSS SECTION [mb]	
37.4 ± 0.7	6.66 ± 0.35	PSI
37.4 ± 0.9	7.16 ± 0.37	PSI
37.8 ± 0.7	6.56 ± 0.34	PSI
38.5 ± 0.7	6.29 ± 0.32	PSI
38.5 ± 0.7	6.25 ± 0.35	PSI
38.6 ± 0.7	6.36 ± 0.37	PSI
38.7 ± 0.7	6.23 ± 0.32	PSI
38.8 ± 0.9	6.64 ± 0.35	PSI
39.3 ± 0.7	6.19 ± 0.35	PSI
39.4 ± 0.9	6.53 ± 0.33	PSI
39.6 ± 0.9	6.69 ± 0.36	PSI
40.2 ± 0.6	5.92 ± 0.38	PSI
40.3 ± 0.6	5.96 ± 0.31	PSI
40.4 ± 0.9	6.53 ± 0.34	PSI
40.6 ± 0.6	5.94 ± 0.31	PSI
40.7 ± 0.6	5.85 ± 0.32	PSI
41.6 ± 0.9	6.16 ± 0.32	PSI
41.7 ± 0.6	5.64 ± 0.34	PSI
42.0 ± 0.6	5.57 ± 0.31	PSI
42.4 ± 0.6	5.58 ± 0.29	PSI
42.4 ± 0.6	5.61 ± 0.30	PSI
43.6 ± 0.9	6.00 ± 0.31	PSI
43.7 ± 0.9	5.98 ± 0.31	PSI
44.2 ± 0.6	5.19 ± 0.27	PSI
44.2 ± 0.6	5.20 ± 0.29	PSI
44.2 ± 0.6	5.25 ± 0.28	PSI
44.2 ± 0.6	5.28 ± 0.27	PSI
44.2 ± 0.9	5.85 ± 0.30	PSI
44.6 ± 0.6	5.17 ± 0.27	PSI
44.6 ± 0.6	5.20 ± 0.29	PSI
45.2 ± 0.9	5.74 ± 0.30	PSI
45.4 ± 0.9	5.71 ± 0.29	PSI
45.5 ± 0.9	5.64 ± 0.29	PSI
45.7 ± 0.8	5.60 ± 0.29	PSI
45.9 ± 0.9	5.64 ± 0.29	PSI
46.7 ± 0.9	5.56 ± 0.29	PSI
47.1 ± 0.9	5.47 ± 0.28	PSI
47.3 ± 0.9	5.42 ± 0.28	PSI
47.4 ± 0.8	5.42 ± 0.29	PSI
48.7 ± 0.8	5.27 ± 0.27	PSI
48.8 ± 0.8	5.19 ± 0.27	PSI
49.0 ± 0.8	5.19 ± 0.27	PSI
49.2 ± 0.8	5.14 ± 0.27	PSI
49.3 ± 0.8	5.17 ± 0.26	PSI
50.4 ± 0.8	5.08 ± 0.26	PSI
50.9 ± 0.8	4.92 ± 0.26	PSI
51.0 ± 1.8	5.23 ± 0.54	TSL
51.2 ± 0.8	4.95 ± 0.25	PSI
52.0 ± 0.8	4.91 ± 0.25	PSI
52.2 ± 0.8	4.83 ± 0.25	PSI
52.5 ± 0.8	4.83 ± 0.25	PSI
52.6 ± 0.8	4.86 ± 0.25	PSI
53.4 ± 0.8	4.77 ± 0.25	PSI
53.5 ± 0.8	4.72 ± 0.24	PSI
54.3 ± 0.8	4.58 ± 0.24	PSI
55.0 ± 0.8	4.59 ± 0.24	PSI
55.3 ± 0.8	4.56 ± 0.24	PSI
55.5 ± 0.8	4.46 ± 0.23	PSI
56.0 ± 0.8	4.40 ± 0.23	PSI
56.4 ± 0.8	4.43 ± 0.23	PSI
56.5 ± 0.8	4.38 ± 0.23	PSI
57.0 ± 0.7	4.33 ± 0.23	PSI
57.3 ± 0.7	4.34 ± 0.23	PSI
57.5 ± 0.8	4.30 ± 0.22	PSI
57.6 ± 1.4	3.82 ± 0.39	TSL
58.0 ± 0.7	4.21 ± 0.22	PSI
58.4 ± 0.7	4.21 ± 0.22	PSI
58.7 ± 0.7	4.25 ± 0.22	PSI
58.8 ± 0.7	4.16 ± 0.21	PSI
59.5 ± 0.7	4.05 ± 0.21	PSI
59.5 ± 0.7	4.12 ± 0.22	PSI
60.6 ± 0.7	4.07 ± 0.21	PSI
60.9 ± 0.7	3.98 ± 0.21	PSI
60.9 ± 0.7	3.93 ± 0.20	PSI
61.7 ± 0.7	3.89 ± 0.20	PSI
62.3 ± 0.7	3.86 ± 0.20	PSI
62.3 ± 0.7	3.91 ± 0.20	PSI
62.6 ± 0.7	3.86 ± 0.20	PSI
63.1 ± 0.7	3.85 ± 0.20	PSI
63.3 ± 0.7	3.80 ± 0.19	PSI
63.6 ± 0.7	3.78 ± 0.20	PSI
63.6 ± 0.7	3.77 ± 0.19	PSI
64.0 ± 0.7	3.71 ± 0.19	PSI
64.9 ± 0.7	3.70 ± 0.19	PSI
65.5 ± 0.6	3.64 ± 0.19	PSI
65.5 ± 0.7	3.62 ± 0.19	PSI
65.8 ± 0.6	3.59 ± 0.19	PSI
66.0 ± 0.6	3.61 ± 0.19	PSI
66.2 ± 0.6	3.59 ± 0.18	PSI
66.9 ± 0.6	3.49 ± 0.19	PSI
67.4 ± 0.6	3.44 ± 0.18	PSI
67.5 ± 0.6	3.47 ± 0.18	PSI
68.3 ± 0.6	3.39 ± 0.18	PSI
68.5 ± 0.6	3.38 ± 0.17	PSI
68.5 ± 0.6	3.37 ± 0.17	PSI
68.8 ± 0.6	3.32 ± 0.17	PSI
69.2 ± 0.6	3.34 ± 0.17	PSI
69.6 ± 0.6	3.26 ± 0.17	PSI
70.0 ± 0.6	3.24 ± 0.17	PSI
71.4 ± 0.5	3.04 ± 0.16	PSI
71.4 ± 0.5	3.07 ± 0.16	PSI
71.4 ± 0.6	3.06 ± 0.16	PSI
71.4 ± 0.6	3.06 ± 0.16	PSI
71.5 ± 0.5	3.05 ± 0.16	PSI
71.5 ± 0.5	3.01 ± 0.16	PSI
74.0 ± 1.0	2.86 ± 0.29	TSL
85.3 ± 1.1	2.78 ± 0.29	TSL
88.1 ± 0.8	2.46 ± 0.26	TSL
99.9 ± 1.7	2.22 ± 0.26	PSI
101. ± 1.7	2.37 ± 0.21	PSI
111. ± 1.6	2.12 ± 0.18	PSI
111. ± 1.6	2.25 ± 0.24	PSI
121. ± 1.5	1.96 ± 0.17	PSI
121. ± 1.5	1.92 ± 0.19	PSI
131. ± 1.4	1.80 ± 0.16	PSI
131. ± 1.4	2.05 ± 0.33	PSI
140. ± 1.3	1.77 ± 0.16	PSI
140. ± 1.4	1.66 ± 0.21	PSI
148. ± 1.3	1.72 ± 0.25	PSI
149. ± 1.3	1.59 ± 0.14	PSI
158. ± 1.1	1.43 ± 0.14	PSI
158. ± 1.1	1.40 ± 0.28	PSI
226. ± 1.8	0.790 ± 0.077	LNS
271. ± 1.3	0.647 ± 0.069	LNS
338. ± 1.7	0.581 ± 0.062	LNS
375. ± 1.3	0.562 ± 0.063	LNS

Table 6: Cross sections [mb] for the production of ^{36}Cl by proton-induced reactions on Ca, Ti, Mn, Fe, Co, and Ni measured by accelerator mass spectrometry.

ENERGY [MeV]	CROSS SECTION [mb]
Ca(p,4pXn)^{36}Cl	
243. ± 2.	14.0 ± 1.4
286. ± 1.	8.6 ± 0.9
351. ± 2.	13.8 ± 1.9
387. ± 1.	13.9 ± 1.3
800. ± 1.	13.7 ± 1.3
1600. ± 1.	9.3 ± 0.9
Ti(p,6pXn)^{36}Cl	
242. ± 2.	6.7 ± 0.6
285. ± 1.	8.1 ± 0.8
350. ± 2.	10.1 ± 0.9
387. ± 1.	11.4 ± 1.0
1200. ± 1.	16.6 ± 2.5
1600. ± 1.	13.9 ± 2.1
2400. ± 1.	16.4 ± 2.5
Mn(p,9p11n)^{36}Cl	
106. ± 1.	0.04 ± 0.01
140. ± 1.	0.19 ± 0.03
165. ± 1.	0.35 ± 0.03
199. ± 1.	0.64 ± 0.06
239. ± 2.	1.39 ± 0.08
282. ± 1.	2.75 ± 0.13
348. ± 2.	3.75 ± 0.17
386. ± 1.	4.12 ± 0.20
1200. ± 1.	17.1 ± 1.1

ENERGY [MeV]	CROSS SECTION [mb]
Fe(p,10pXn)^{36}Cl	
236. ± 2.	0.87 ± 0.08
237. ± 2.	0.73 ± 0.07
280. ± 1.	1.20 ± 0.11
346. ± 2.	2.28 ± 0.21
800. ± 1.	8.11 ± 0.74
2600. ± 1.	8.54 ± 1.28
Co(p,11pXn)^{36}Cl	
233. ± 2.	0.26 ± 0.02
278. ± 1.	0.62 ± 0.05
344. ± 2.	1.31 ± 0.11
380. ± 1.	1.74 ± 0.14
Ni(p,12pXn)^{36}Cl	
231. ± 2.	1.05 ± 0.09
275. ± 1.	0.65 ± 0.05
341. ± 2.	1.18 ± 0.08
378. ± 1.	1.85 ± 0.15
800. ± 1.	7.16 ± 0.66
1200. ± 1.	8.75 ± 1.32

INSTITUT FÜR KERNCHEMIE
UNIVERSITÄT MAINZ

1. Odd-even and shell effects in the fission of the odd compound nucleus ^{243}Am (Z=95)

P. Stumpf, H. O. Denschlag, H. R. Faust

A first observation of odd-even effects of protons, i.e. the preferential formation of fission products with even atomic numbers among the light fission fragments of an odd-Z compound nucleus have been reported already some time ago [1, 2] by our group. Results on the variation of the odd-even effect as a function of the kinetic energy and of an effect of the 50-neutron shell will be presented in the following.

The measurements were performed at the recoil mass separator Lohengrin of the Institut Laue-Langevin in Grenoble (France) using targets of ^{241}Am that were converted to $^{242m+g}$Am in the target position of the mass separator. The identification of the atomic numbers of the fission products took place in an ionization chamber with a split anode (BIC) [3].

Local odd-even factors were calculated using the "method of the 3rd difference" [4]. The results obtained for protons are shown in Fig. 1 at various kinetic energies of the fragments.

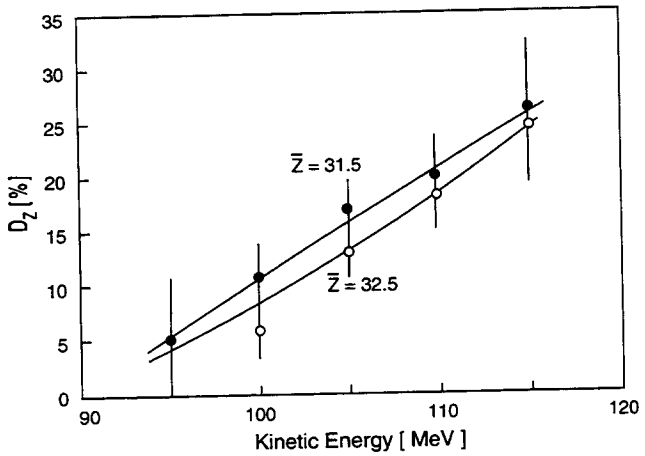

Fig. 1: Local odd-even effect for protons (D_Z [%]) at the mean nuclear charges $\bar{Z}$=31.5 and $\bar{Z}$=32.5 obtained according to [4] from the experimental yield values obtained for specific kinetic energies of the fragments (E_{kin}, corrected for energy loss in the target).

The figure shows an odd-even effect for the mean nuclear charges $\overline{Z}$=32.5 and 31.5, respectively, varying from 5 % for fragments of low kinetic energy up to about 25 % for fragments of high kinetic energy. The size of this odd-even effect is comparable to the effect in correspondingly asymmetric regions of the even-Z compound nuclei, especially if the larger fissility parameter for ^{243}Am is taken into account.

The fact that the odd-even effect increases with the kinetic energy indicates that even-Z nuclei possess a higher kinetic energy than odd ones. The mean kinetic energy of the fission fragments as a function of their atomic number is shown in Fig. 2.

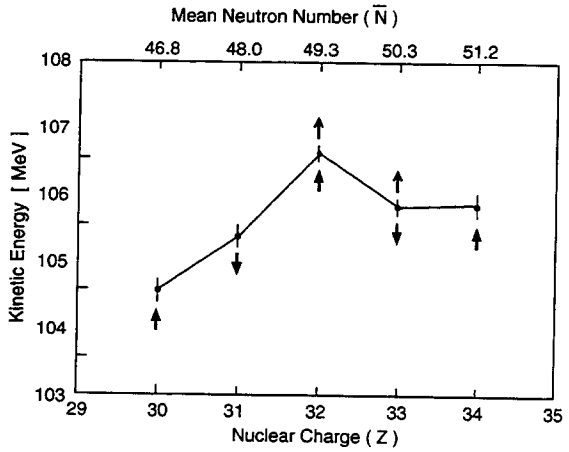

Fig. 2: Mean initial kinetic energy (E_{kin}) of fission fragments as a function of their nuclear charge (Z) and corresponding mean neutron number ($\overline{N}$). The arrows below the data points indicate the direction of the influence of the odd-even effect and the arrows above the data points indicate the direction of a bias due to the effect of the closed 50 neutron shell.

The particularly high kinetic energy of Z = 32 may be due to an additional effect of the neutron shell at N = 50. The present measurements of charge distribution allow to calculate the mean neutron number (mean mass) for any element (any Z). Assuming a value of 0.5 for prompt neutron emission, we obtain a value of $\overline{N}$=49.3 for Z=32 and a value of $\overline{N}$ = 50.3 for Z = 33 (Fig. 2). In consequence, the 50 neutron shell is located between Z=32 and Z=33 presumably producing an increased kinetic energy in both elements. For Z = 32 the odd-even effect adds to the shell effect with a further increase of E_{kin}, wheras for Z = 33 the (negative) odd-even effect is opposed to the shell effect compensating its effect on E_{kin}. The observed behaviour can therefore be interpreted as a superposition of odd-even and shell effects.

In summary, we conclude that we observe odd-even and shell effects in the very asymmetric fission of the odd-Z nucleus ^{243}Am. With the limited information available so far, it is difficult to disentangle the contribution of the shell effect to D_Z calculated above. In this sense the value of D_Z given represents an upper limit of the true odd-even effect.

The odd-even effects observed in very asymmetric fission are different from those in the standard high yield regions: Odd-even effects in the high yield region are limited to even compound nuclei and are not observed e.g. in the fission of the odd nucleus ^{237}Np [5]. In contrast, odd-even effects in the very asymmetric fission are comparable in size for both even and odd compound systems. This observation seems to indicate a different mechanism responsible for the two effects. Further discussion of this work will be found in Ref. [6].

Acknowledgement: This work was supported by the Bundesministerium für Forschung und Technologie under contract No. 06-MZ-465 and 06-MZ-476.

References

1. P. Stumpf, U. Güttler, H. O. Denschlag, H. R. Faust: Odd-Even Effects in the Reaction $^{241}Am(2n,f)$, in S. Cierjacks (Ed.) Progress Report on Nuclear Data Research in the Federal Republic of Germany, Report NEANDC(E)-322-U, Vol. V, INDC(Ger)-36/LN+Special, KfK 4953 (1991)
2. P. Stumpf, U. Güttler, H. O. Denschlag, H. R. Faust: Odd-Even Effects in the Reaction $^{241}Am(2n,f)$, in (S.M. Qaim, Ed.) Nuclear Data for Science and Technology, Springer Verlag, Berlin (1992), p. 145
3. J. P. Bocquet, R. Brissot, H. R. Faust; Nucl. Instr. Methods in Phys. Res. A267, 466-472 (1988)
4. B. L. Tracy, J. Chaumont, R. Klapisch, J. M. Nitschke, A. M. Poskanzer, E. Roeckl, C. Thibault; Phys. Rev. C5, 222 (1972)
5. G. Martinez, G. Barreau, A. Sicre, T. P. Doan, P. Audouard, B. Leroux, W. Arafa, R. Brissot, J. P. Bocquet, H. Faust, P. Koczon, M. Mutterer, F. Gönnenwein, M. Asghar, U. Quade, K. Rudolph, D. Engelhardt, E. Piasecki; Nucl. Phys. A515, 433-465 (1990)
6. P. Stumpf, H. O. Denschlag, H. R. Faust: Odd-even effects in the fission of the odd compound nucleus ^{243}Am (Z=95), in C. Wagemans (Ed.) Proceedings Seminar on Fission, Pont d'Oye III, May 1995, preprints available from H.O.D., Inst. f. Kernchemie, Universität, D-55099 Mainz.

INSTITUT FÜR KERNCHEMIE
PHILIPPS-UNIVERSITÄT MARBURG

^{252}Cf: Direct Determination of Partial Neutron Multiplicities in Correlation with Fission-Fragment Mass and Energy

K. Siemon, R.A. Esterlund, J. van Aarle, W. Westmeier and P. Patzelt

Although the spontaneous-fission properties of ^{252}Cf have been studied for well over 35 years [1], many interesting and informative details continue to come to light. In a recent publication [2] by our group, correlations of neutron-multiplicities with fission fragment mass and energy were presented, whereby assignments of the corresponding partial neutron multiplicities were deduced by using the measured total neutron multiplicities together with the aid of the well-known "saw-tooth" average neutron multiplicity distribution as a function of fission-fragment mass [3]. In this work, the *partial* neutron multiplicities have now been measured *directly* as a function of fission-fragment mass and energy. This assignment of neutrons to one of the fission fragments is achieved *via* separate counter electronics for the two divided halves of the neutron sphere. The fission-fragment detectors are placed in such a manner that they preferentially select those events whose vectors point well into the semi-spheres, thus achieving the greatest efficiency for neutrons from a given fission fragment to be registered in their corresponding semi-sphere and *vice-versa*. Moreover, these new data have been corrected in such a way so as to eliminate non-full-energy events.

A detailed description of the neutron sphere detector used for the measurements is given elsewhere [2,4,5]. In many previous works [2,3,6,7] where neutron multiplicities are indirectly assayed with a high-efficiency liquid-scintillation counter, the procedure suffers from two disadvantages: 1) if one or more of the γ-rays associated with neutron capture in one semi-sphere enters the other semi-sphere and is detected there, coincident registration of one neutron in each semi-sphere will occur (cross-talk); 2) if the velocity vector of a neutron is lar-

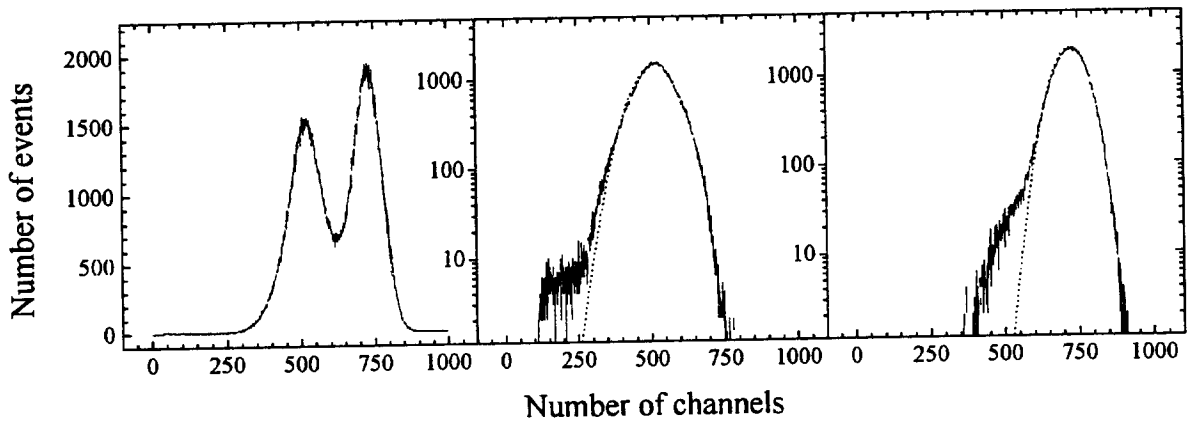

Fig. 1: Kinetic energy spectra for ^{252}Cf (see text).

ger than and oriented opposite to the corresponding fission-fragment velocity vector, then the neutron corresponding to one semi-sphere will in fact be registered in the other semi-sphere, thus being correlated with the wrong fission fragment. In the present experiment, events with γ-ray cross-talk (point 1) have been correctly sorted by using a special fast-logic veto circuit.

Fig. 1 depicts pulse-height spectra for one of the neutron-sphere halves. The leftmost section shows data for all fragment masses, the center section shows the data corresponding to heavy-fission fragments and the rightmost section displays data for the light partners. The peak-to-valley ratios at the left have good values of 2.19 and 2.76. The dotted lines in the center and rightmost sections designate gaussian functions fitted to the low-energy portions of the distributions. Events occurring with pulse-height values located to the left of the fitted gaussian function were regarded as corresponding to non-full-energy events and correspondingly discarded from the data base. This method of eliminating events with energy losses due to scattering "cleanses" the data, as shown in Fig. 2, where primary mass distributions constructed with the *experimental* partial neutron multiplicity values are depicted. The uppermost portion of the figure depicts the mass yields summed over all neutron multiplicities. The peak-to-valley ratio here is 16.1:1. The center and lower sections display the mass yields corresponding to various total neutron multiplicities in the ranges $0 \leq \nu \leq 3$ and $4 \leq \nu \leq 7$. The data points at very large mass asymmetry in the uppermost part of the figure arise from non-full-energy events, which otherwise have been eliminated from the rest of the mass-yield data. In a similar manner. Fig. 3 depicts the corresponding primary TKE distributions. As in Fig. 2, the leftmost part of the figure displays data summed over all neutron multiplicities, whereas the center and right portions depict data for $0 \leq \nu \leq 3$ and $4 \leq \nu \leq 7$, respectively. The data points in the leftmost portion of the figure also show the data resulting from non-full-energy events, which have been removed from the other TKE data. The average primary TKE obtained from these data is

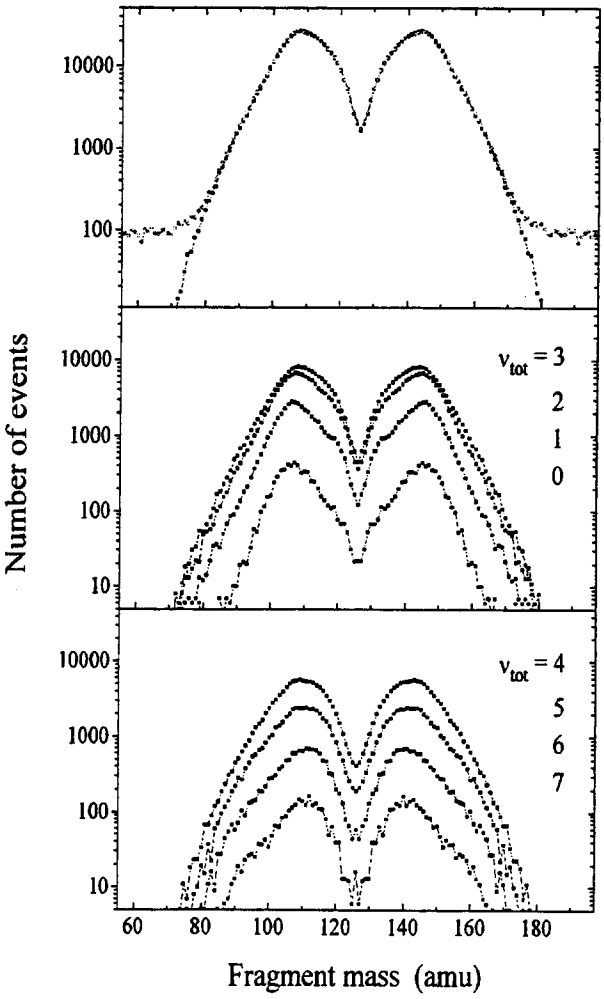

Fig. 2: Mass yields for ^{252}Cf (see text).

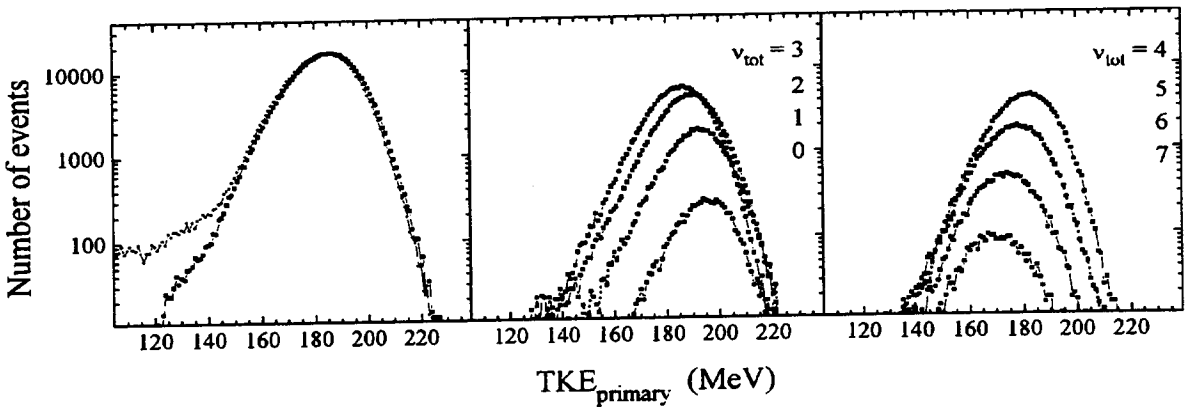

Fig. 3: Primary TKE spectra for ^{252}Cf (see text).

183.90 ± 0.27 MeV (secondary TKE = 180.94 ± 0.26 MeV), which compares very well with the recommended [8] value of 184.1 MeV. Finally, in Fig. 4, we show raw data for our average partial neutron multiplicity against fragment mass and TKE. The data resemble the well-known saw-tooth [3] distribution for ^{252}Cf, but here there have been no corrections for dead time, background events and counting efficiency, as well as registering of neutrons in the wrong semi-sphere (point 2 above). Perhaps the most interesting feature of this distribution is the prominent sharp peak located at high kinetic energy. Because of poor statistics (especially on the edges of the distribution, where only single events have been registered), it was necessary to smooth these data. In the future, we expect to have accumulated enough events such that the data will become more physically definitive.

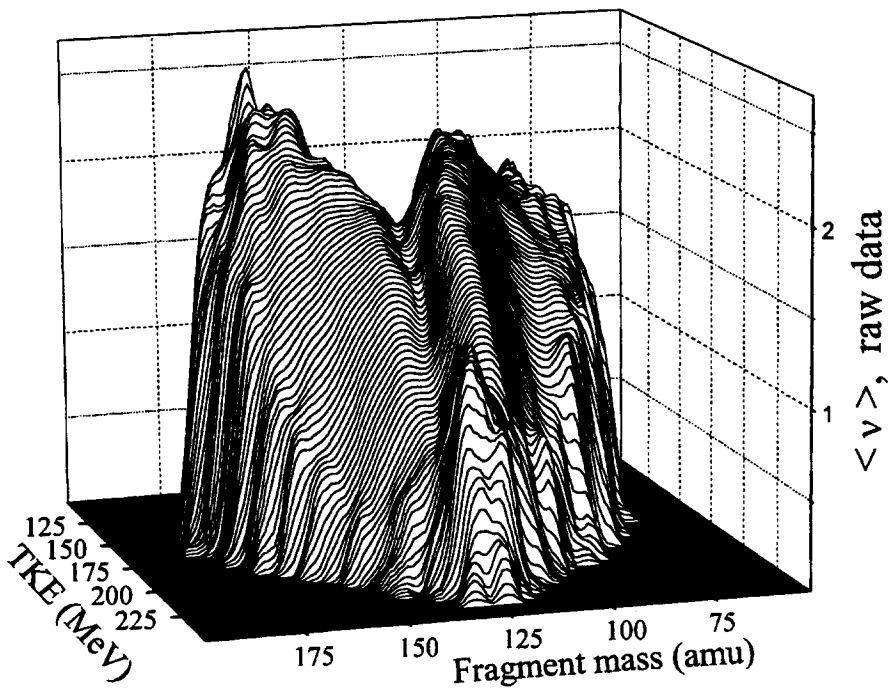

Fig. 4: Partial neutron multiplicity vs. fragment mass vs. TKE (raw data - see text).

References

[1] See, *e.g.*, S.L. Whetstone Jr.: Prompt-Neutron Emission from Single Fission Fragments, Phys. Rev. 114 (1959) 581

[2] J. van Aarle, W. Westmeier, R.A. Esterlund and P. Patzelt: ^{252}Cf: Neutron Multiplicities in Correlation with Fission-Fragment Mass and Energy, Nucl. Phys. A578 (1994) 77, as well as in: Progress Report on Nuclear Data Research in the Federal Republic of Germany, NEA/NSC/DOC(94)21, ed. S.M. Qaim (Aug. 1994) 43

[3] C. Budtz-Jørgensen and H.-H. Knitter: Simultaneous Investigation of Fission Fragments and Neutrons in ^{252}Cf (SF), Nucl. Phys. A490 (1988) 307

[4] J.F. Wild, J. van Aarle, W. Westmeier, R.W. Lougheed, E.K. Hulet, K.J. Moody, R.J. Dougan, E.-A. Koop, R.E. Glaser, R. Brandt and P. Patzelt: Prompt Neutron Emission from the Spontaneous Fission of ^{260}Md, Phys. Rev. C41 (1990) 640

[5] J. van Aarle: Untersuchungen zur Spontanspaltung von ^{260}Md und ^{252}Cf (Doctoral thesis, Universität Marburg, 1992, unpublished)

[6] See, *e.g.*, I. Düring, U. Jahnke and H. Märten: Fragment-Neutron and Neutron-Neutron Correlations in ^{252}Cf Spontaneous Fission, Progress Report on Nuclear Data Research in the Federal Republic of Germany, NEA/NSC/DOC(94)21, ed. S.M. Qaim (Aug. 1994) 19

[7] See, *e.g.*, I. Düring, M. Adler, H. Märten, A. Ruben, B. Cramer and U. Jahnke: Multi-fold Correlations Between ^{252}Cf (sf) Fragments and Fission-Neutron γ-Rays, in Proceedings of the International Workshop on High-Resolution Spectroscopy of Fission Fragments, Neutrons and γ-Rays, FZR 93 - 08, eds. H. Märten and K.D. Schilling (Mar. 1993) 103

[8] F. Gönnenwein: Mass, Charge, and Kinetic Energy of Fission Fragments, in The Nuclear Fission Process, ed. C. Wagemans (CRC Press, Boca Raton, 1991) p. 323

PHYSIKALISCH-TECHNISCHE BUNDESANSTALT BRAUNSCHWEIG

1. Neutron Data

1.1 Elastic Scattering Cross Sections from Natural Lead

D. Schmidt, W. Mannhart, Xia Haihong*

Lead is discussed as a candidate for neutron multiplication in fusion reactors. Elastic scattering data are scarce in the energy region below 14 MeV. Some measurement reports have been published, but only at energies near 8, 9, 11 and 14 MeV.

Measurements have been carried out at seven energies between 7.97 MeV and 14.31 MeV in steps of about 1 MeV. The data reduction process is outlined in detail elsewhere [1]. The agreement in shape of the calculated TOF spectra with the measured ones was substantially improved by a new folding procedure [2]. The number of measured angles was between 35 and 40, corresponding to an angle distance of about the standard deviation of the angle distribution density, following from Monte Carlo calculations.

Fig. 1 shows the comparison of our measurement at 14.31 MeV with data from the literature [3-8]. The ratio of those data to the Legendre polynomial fit to our measurement is illustrated. With the exception of one data set [4], the agreement is good . Two other data sets [9,10] are not included, as there are deviations of up to a factor of about 3.

The deviation of the ENDF/B-VI evaluation from our measurement is considerable. The same applies to the angle-integrated cross sections of the ^{208}Pb isotope. A new evaluation is recommended for these data.

The data reduction was also completed using an analytical approach [11]. Here, the angle-integrated cross section and the Legendre polynomial coefficients are corrected. The results of this semi-empirical method were compared with those of our processing, where realistic Monte Carlo calculations of the TOF spectra are fitted to the measured ones at all angles simultaneously. After some iteration steps this procedure converges. The differences of the two methods were between ± 10% and ± 20%, but in deep minima even larger. This

* Permanent address: CIAE, Beijing, P.R. China

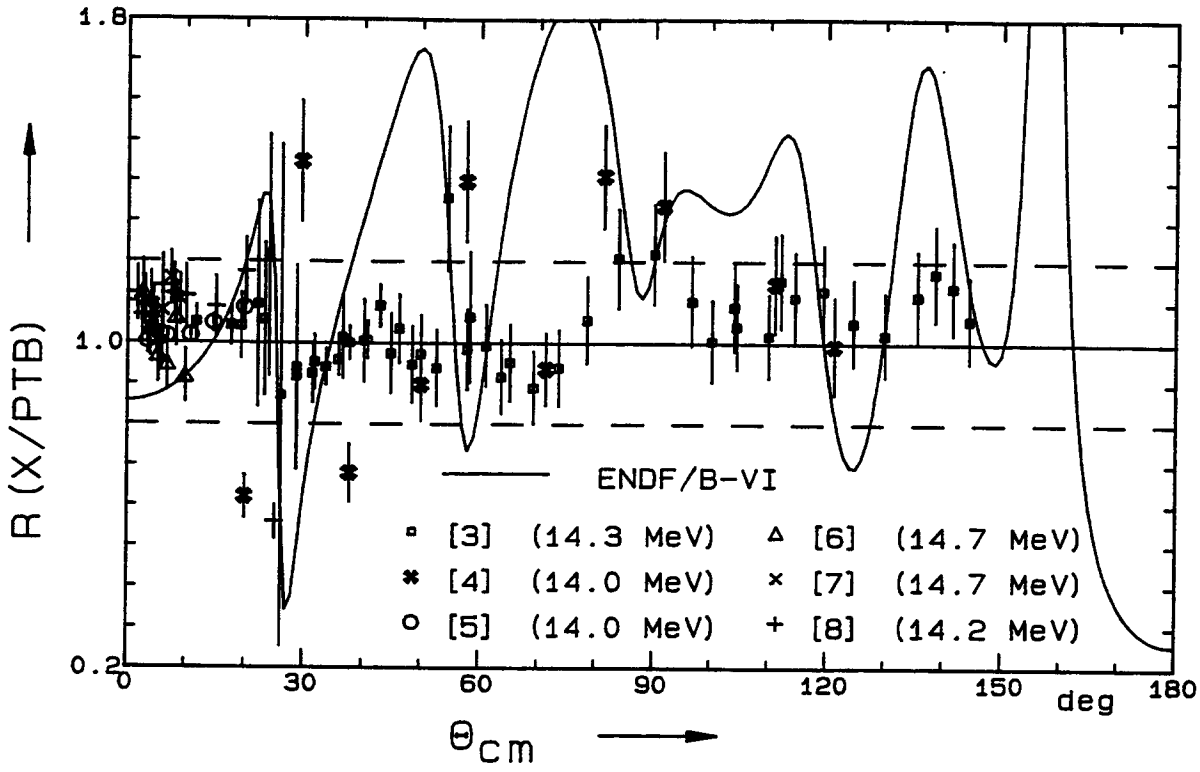

Fig. 1 Ratio of elastic cross sections from natural lead from the literature [3-8] to the Legendre polynomial fit to our data measured at 14.31 MeV; the comparison with the evaluation ENDF/B-VI is included.

demonstrates the shortcomings of the analytical method if large gradients in the angular distributions occur.

The data analysis is continued to extract double-differential cross sections. The first step necessary is to subtract the scattered breakup neutrons that are also simulated in the MC calculation. The data for this simulation are adjusted by a comparison with measurements using a pure breakup neutron source from the ^{4}He(d,n) reaction [12]. A detailed analysis of this method is being studied.

1.2 Measurement of Activation Cross Sections between 8 and 14 MeV

W. Mannhart, D. Schmidt, Xia Haihong*

The database of activation cross sections in the neutron energy range between 10 and 13.5 MeV is scanty, one reason being the lack of a real monoenergetic neutron source

applicable to this energy range. A convenient neutron source is the D(d,n)^{3}He reaction provided the breakup neutrons of the D(d,np) channel can be properly corrected. Alternate neutron sources exist with the reactions H(t,n), H(^{7}Li,n), H(^{11}B,n), ^{3}He(^{12}C,n) and ^{14}N(d,n). However, common to all these sources is a relatively large energy width and, with the exception of H(t,n), a low neutron intensity. The application of the H(t,n) reaction is further complicated by the necessity of a triton beam.

In view of these complications, at the PTB the potential of the D(d,n) reaction has carefully been investigated. Based on detailed measurements of the D(d,np) breakup neutron spectra [13], the D(d,n)^{3}He neutron source is now routinely used for activation cross section measurements between 8 and 14 MeV neutron energy. Deuterons are accelerated with the PTB compact cyclotron CV28 and interact with a 3 cm long deuterium gas target. Samples are placed at zero degrees at distances of 4-10 cm from the gas target. The neutron fluence is chiefly monitored with a ^{238}U(n,f) fission chamber. The radioactivity induced is counted with a Ge(Li) or HPGe detector. A list of the neutron reactions already measured is given in table 1. The result of a typical measurement is shown in Fig. 2.

Table 1: Activation cross section measurements performed at the PTB

Reaction	Energy range (in MeV)	Number of energies	Reference
^{24}Mg(n,p)^{24}Na	8.3 - 14.7	26	[14]
^{27}Al(n,α)^{24}Na	8.3 - 14.7	26	[14]
^{54}Fe(n,p)^{54}Mn	9.1 - 14.6	13	[15]
^{54}Fe(n,α)^{51}Cr	9.1 - 14.6	13	[15]
^{56}Fe(n,p)^{56}Mn	9.1 - 14.6	13	[15]
^{58}Ni(n,p)^{58}Co	8.5 - 13.5	15	[16]
^{59}Co(n,p)^{59}Fe	8.0 - 14.3	19	[17]
^{59}Co(n,α)^{56}Mn	8.0 - 14.3	19	[17]
^{59}Co(n,2n)$^{58m+g}$Co	11.0 - 14.3	13	[17]
^{93}Nb(n,2n)^{92m}Nb	9.1 - 13.5	14	[16]
^{103}Rh(n,n')^{103m}Rh	5.7 - 12.0	14	[18]

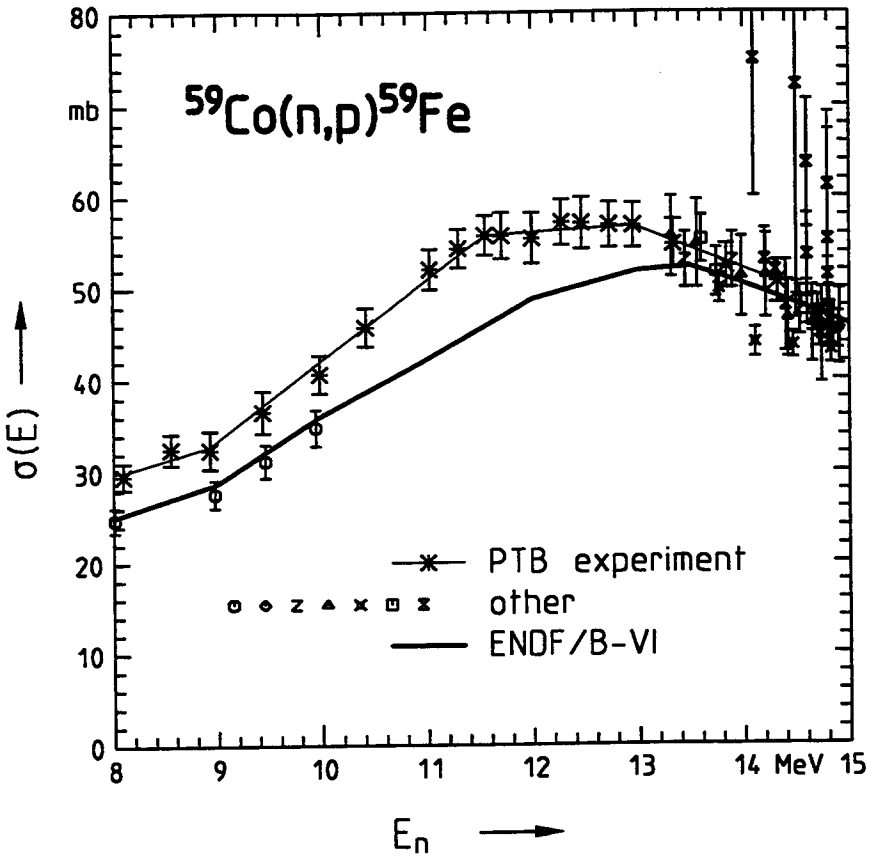

Fig. 2 Complete database of the ^{59}Co(n,p)^{59}Fe reaction between 8 and 15 MeV.

Without the PTB experiment, the database of the ^{59}Co(n,p)^{59}Fe reaction, shown in Fig. 2 comprises a single experiment below 10 MeV and a variety of (often slightly divergent) measurements above 13.3 MeV. The ENDF/B-VI evaluation followed the low energy experiment and the cross section up to the 14 MeV region was extrapolated. The recent PTB experiment shows that below 13 MeV the ^{59}Co(n,p) cross section is strongly underestimated (by about 17%). Above 13 MeV there is a convergence of the PTB experiment and the previous ENDF/B-VI evaluation.

1.3 Validity of the Correction for D(d,np) Breakup Neutrons in Activation Measurements

W. Mannhart, D. Schmidt, Xia Haihong*

When the D(d,n)^{3}He reaction is used for the production of neutrons between 8 and 14 MeV in activation experiments, the main corrections in the data analysis are the 'gas-out' effect and the correction for breakup neutron contributions. Both corrections strongly increase with the neutron energy and also depend in their magnitude on the reaction threshold

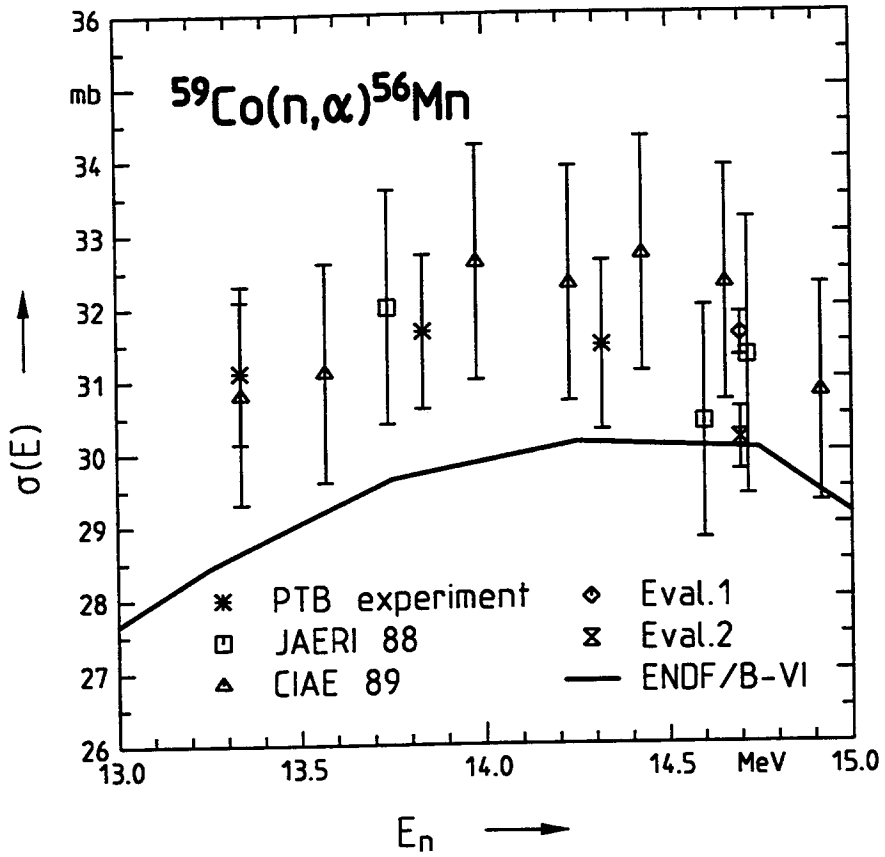

Fig. 3 Cross section of the $^{59}Co(n,\alpha)^{56}Mn$ reaction around 14 MeV.

energy. The first correction can be experimentally determined, whereas the breakup correction requires an analytical treatment. For the $^{238}U(n,f)$ reaction, commonly used as neutron fluence monitor, with a relatively low threshold the breakup correction is of the order of 50% at 14 MeV neutron energy, meaning that only half of the fission rate is from monoenergetic 14 MeV neutrons. The correction is done by folding the specific excitation function with the angle-dependent and experimentally measured [13] breakup neutron spectra of the D(d,n) reaction. However, corrections of such an order of magnitude require additional confirmation of their validity. Around 14 MeV, in the region of maximum breakup corrections with the D(d,n) neutron source, cross section measurements performed with a $T(d,n)^4He$ neutron source serve as a benchmark. Fig. 3 gives an example.

In Fig. 3 the PTB measurements of the $^{59}Co(n,\alpha)$ cross section based on a D(d,n) neutron source are compared with measurements from JAERI [19] and CIAE [20] based on a T(d,n) neutron source. Besides the measurements the result of two evaluations of 14 MeV data [21,22] is also shown. It can be seen that ENDF/B-VI confirms the value of the 14 MeV evaluation no. 2 [22]. Due to the $^{238}U(n,f)$ neutron monitor reaction applied, the PTB data

comprise breakup corrections of between 44% at 13.34 MeV and 50% at 14.32 MeV. The fair agreement of the PTB data with that from JAERI and CIAE is a clear confirmation of the correctness of the breakup corrections applied in the PTB experiment, and substantiates the validity of these corrections below 14 MeV where such tests are impossible. Similar comparisons with other measured neutron reactions are given elsewhere [15,17].

2. Radionuclide Data

2.1 Half-Lives

H. Siegert, U. Schötzig

1. The gamma emissions from an aqueous solution of the radionuclides ^{121}Te and ^{121}Te^{m} were followed simultaneously with an HPGe detector over a period of about 120 days. A revised value for the half-life

$$T_{1/2}(^{121}\text{Te}) = (19.16 \pm 0.05)\ \text{d}$$

is deduced, and differs appreciably from the value of 16.8 d adopted in the literature. A full description of the evaluation procedure will be published in Appl. Radiat. Isot. (1995).

2. The half-life of ^{55}Fe was determined by performing 30 count-rate measurements of 3 point sources with a Si(Li) detector during a period of about 1800 days, resulting in a value of

$$T_{1/2}(^{55}\text{Fe}) = (1003 \pm 3)\ \text{d}$$

which is in agreement with the evaluated value of (999 ± 8) d, documented in IAEA-TECDOC-619 (1991).

References

[1] D. Schmidt et al.: Report PTB-N-20, PTB Braunschweig/FRG (1994)

[2] D. Schmidt et al.: "Analysis of the Shape of Neutron TOF Lines", to be published

[3] J.H. Coon et al.: Phys. Rev. **111** (1958) p. 250

[4] W. Stelson et al.: Nucl. Phys. **68** (1965) p. 97

[5] W. Bucher et al.: Nucl. Instr. Meth. **111** (1973) p. 237

[6] Cao Jinhua et al.: EXFOR 32518, IAEA Vienna (1985)

[7] Qi Huei-Quan et al.: Report INDC(CPR)-006/L, IAEA Vienna (1985)

[8] Li Jingde et al.: EXFOR 30762, IAEA Vienna (1987)

[9] B.Ya. Guzhovski: EXFOR 40643, IAEA Vienna (1961)

[10] L.A. Rayburn: Phys. Rev. **116** (1959) p. 1571

[11] C.A. Engelbrecht: Nucl. Instr. Meth. **93** (1971) p. 103

[12] D. Schmidt et al.: Report PTB-N-18, PTB Braunschweig/FRG (1994)

[13] S. Cabral, G. Börker, H. Klein, W. Mannhart: Nucl. Sci. Engn. **106** (1990) p. 308

[14] G. Börker, H. Klein, W. Mannhart, M. Wagner, G. Winkler: Nuclear Data for Science and Technology, (S. Igarasi ed.), Saikon Publ. Comp., Tokyo (1988) p. 1025

[15] J.W. Meadows, D.L. Smith, L.R. Greenwood, L.P. Geraldo, W. Mannhart, G. Börker: Nuclear Data for Science and Technology, (S.M. Qaim ed.), Springer Verlag, Berlin (1992) p. 288

[16] D.L. Smith, J.W. Meadows, H. Vonach, M. Wagner, R.C. Haight, W. Mannhart: Nuclear Data for Science and Technology, (S.M. Qaim ed.), Springer Verlag, Berlin (1992) p. 282

[17] W. Mannhart, D. Schmidt, Xia Haihong: Nuclear Data for Science and Technology, (J.K. Dickens ed.), American Nuclear Society, La Grange Park (1994) p. 285

[18] M.M.H. Miah, H. Vonach, W. Mannhart, D. Schmidt: Nuclear Data for Science and Technology, (J.K. Dickens ed.), American Nuclear Society, La Grange Park (1994) p. 278

[19] Y. Ikeda at al.: Report JAERI-1312, Japan Atomic Energy Research Institute (1988)

[20] Zhao Wenrong et al.: Report INDC(CPR)-16/L, IAEA Vienna (1989)

[21] T.B. Ryves: European App. Res. Rept. - Nucl. Sci. Techn. **7** (1989) p. 1241

[22] B.P. Evain: Report ANL/NDM-89, Argonne National Laboratory (1985)

APPENDIX

Addresses of Contributing Laboratories

Institut für Kernphysik III
Director: Prof. Dr. G. Schatz
Senior reporter: Dr. F. Käppeler
Forschungszentrum Karlsruhe
Postfach 36 40
76021 Karlsruhe

Institut für Neutronenphysik
und Reaktortechnik
Director: Prof. Dr. G. Kessler
Senior reporter: Dr. F.H. Fröhner
Forschungszentrum Karlsruhe
Postfach 36 40
76021 Karlsruhe

Institut für Nuklearchemie
Director: Prof. Dr. G. Stöcklin
Senior reporter: Dr. S.M. Qaim
Forschungszentrum Jülich
Postfach 1913
52425 Jülich

Institut für Kern- und Teilchenphysik
Director: Prof. Dr. K.R. Schubert
Senior reporter: Prof. Dr. K. Seidel
Technische Universität Dresden
Mommsenstr. 13
01062 Dresden

Zentrum für Strahlenschutz und Radioökologie
Head and senior reporter: Prof. Dr. R. Michel
Universität Hannover
Am Kleinen Felde 30
30167 Hannover

Abteilung Nuklearchemie
Director: Prof. Dr. G. Stöcklin
Senior reporter: Dr. U. Herpers
Universität zu Köln
Otto-Fischer-Straße 12 - 14
50674 Köln

Institut für Kernchemie
Head and senior reporter: Prof. Dr. H.O. Denschlag
Universität Mainz
Fritz-Strassmann-Weg 2
55128 Mainz

Fachbereich Physikalische Chemie
Kernchemie
Senior Reporter: Prof. Dr. P. Patzelt
Philips-Universität Marburg
Lahnberge
35043 Marburg/Lahn

Physikalisch-Technische Bundesanstalt
Abteilung 7, Neutronenphysik
Director: Prof. Dr. R. Jahr
Senior reporter: Dr. W. Mannhart
Bundesallee 100
38116 Braunschweig